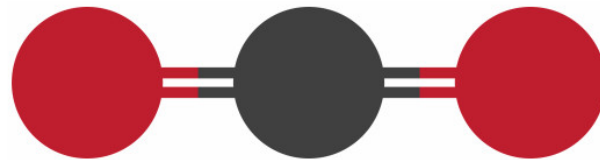


**UNIVERSITY  
OF TWENTE.**

Study of water adsorption  
on an amine adsorbent for  
**Direct Air Capture of CO<sub>2</sub>**

By **Juan García Martínez**  
March 2, 2020



---

Master of Science Thesis on Chemical Engineering  
Faculty of Science and Technology (TNW)  
Sustainable Process Technology group (SPT)

---

#### ASSESSMENT COMMITTEE

|                         |                           |
|-------------------------|---------------------------|
| <i>Daily supervisor</i> | Ir. H.M. Schellevis       |
| <i>Committee member</i> | Dr. ir. D.W.F. Brillman   |
| <i>Chairman</i>         | Prof. dr. S.R.A. Kersten  |
| <i>External member</i>  | Prof. dr. ir. L. Lefferts |

## Acknowledgements

I would like to offer my most sincere gratitude to Michel and Wim for their inestimable help, valuable time, enthusiasm and active supervision. They made me feel that we were all working together as a team. Big thanks also to all the good friends that supported me throughout this time, particularly Jeffrey, Mohammad, Andrea, Mari, Styrmir, Alessandro, Simone, Monica and the Dutch dudes (you know who you are). It would not have been the same without you all.

Finalmente, no puedo dejar de dar las gracias a mis queridos amigos de Tarancón, sin los cuales no se que haría. Y por supuesto a mi madre Montse, porque sin su apoyo no habría llegado a ninguna parte, ella es la que ha hecho todo esto posible.

### Abstract

To limit the negative consequences of climate change on the environment, negative emissions of CO<sub>2</sub> will likely be needed. One way to reach them is via the use of Direct Air Capture (DAC) technologies. A promising technology is the use of solid amine sorbents via a low temperature sorbent DAC process. One such process is being developed by the SPT department, and a key issue is the co-adsorption of atmospheric water vapor, because it increases the energy demand of the process. This work is focused on the characterization of several aspects of water adsorption over an amine adsorbent material (Lewatit VP OC 1065<sup>TM</sup>) which is being studied as the benchmark for the process.

Two methods were used to measure the equilibrium water adsorption capacity under different conditions of Relative Humidity (RH) and temperature. First, the method used by Veneman et al.[1], based on the measurement of water breakthrough curves. After several experiments and extensive testing, it was concluded that the method is too imprecise, inaccurate and inconsistent. Previously published literature data published may also be subject to these problems. The second method, based on gravimetric measurements, was developed to overcome the shortcomings of the first and determined to be sufficiently precise and consistent. Additionally, an improved gravimetric method is described and recommended for use in further research.

The equilibrium capacity measurements show a Type V adsorption isotherm behavior with a temperature dependence and an energetically weak interaction between adsorbate and adsorbent. The GAB isotherm was selected to develop a temperature dependent isotherm model of the system. This is the main output of this work and describes the system well at the relevant ranges of humidity (5-85%) and temperature (5-35°C). The adsorption heat of water over Lewatit was estimated to be on the range of  $\Delta H_{ads,W} = (63 - 50)$  kJ/mol. Hysteresis experiments showed an outstandingly wide hysteresis loop, in contrast with expectations from previous literature[1] and analyses of pore condensation in the material. This behavior could have significant implications for process operation.

Finally, the energy requirements of the DAC process were estimated. Operation at low values of RH minimizes energy use, so arid climates are recommended. To produce pure CO<sub>2</sub> from ambient air using steam as purge gas for regeneration of the sorbent, lower temperatures result in reduced energy consumption.

# Contents

|          |   |           |
|----------|---|-----------|
| <b>1</b> | <b>Introduction and scope</b>   | <b>1</b>  |
| 1.1      | Problem background . . . . .  | 1         |
| 1.2      | Direct air capture of CO <sub>2</sub> on amine adsorbents . . . . .   | 3         |
| 1.3      | Low temperature solid sorbent DAC process . . . . .                   | 3         |
| 1.4      | Problem definition . . . . .  | 4         |
| 1.5      | Research goals . . . . .  | 4         |
| <b>2</b> | <b>Literature study</b>   | <b>6</b>  |
| 2.1      | Water adsorption over Lewatit . . . . .                               | 6         |
| 2.2      | Adsorption isotherm . . . . .   | 6         |
| 2.2.1    | Isotherm classification . . . . .                                     | 7         |
| 2.2.2    | Water isotherm model . . . . .  | 7         |
| 2.3      | Adsorption hysteresis . . . . .                                       | 10        |
| <b>3</b> | <b>Materials and methods</b>  | <b>12</b> |
| 3.1      | Lewatit VP OC 1065 . . . . .  | 12        |
| 3.2      | Breakthrough method . . . . .   | 13        |
| 3.3      | Gravimetric method . . . . .  | 18        |
| <b>4</b> | <b>Results and discussion</b>   | <b>20</b> |
| 4.1      | Experimental methods validation . . . . .                             | 20        |
| 4.2      | Gravimetric data discussion . . . . .                                 | 23        |
| 4.3      | Isotherm model . . . . .  | 25        |
| 4.3.1    | Experimental fit results and isotherm model selection . . . . .       | 25        |
| 4.3.2    | Temperature dependent model . . . . .                                 | 28        |
| 4.4      | Adsorption hysteresis . . . . .                                       | 31        |
| 4.5      | Process design considerations . . . . .                               | 33        |
| <b>5</b> | <b>Conclusions and recommendations</b>                                | <b>38</b> |
| 5.1      | Conclusions . . . . .   | 38        |
| 5.2      | Recommendations . . . . .   | 38        |
|          | <b>References</b>   | <b>39</b> |
|          | <b>List of Symbols</b>  | <b>42</b> |
| <b>A</b> | <b>Appendices</b>   | <b>43</b> |
| A.1      | Review of supported sorbents for CO <sub>2</sub> adsorption . . . . . | 43        |
| A.1.1    | Metal oxide supported amine sorbents . . . . .                        | 43        |
| A.1.2    | Organic solid supported amine sorbents . . . . .                      | 43        |
| A.1.3    | Metal organic frameworks . . . . .                                    | 44        |
| A.1.4    | Material Selection . . . . .  | 44        |
| A.2      | CO <sub>2</sub> adsorption mechanism . . . . .                        | 44        |
| A.2.1    | Possible mechanisms . . . . .   | 44        |
| A.2.2    | Mechanism in Lewatit . . . . .  | 45        |
| A.3      | Response time deconvolution analysis . . . . .                        | 45        |
| A.4      | Process design parameters . . . . .                                   | 47        |
| A.5      | Sensitivity analysis of energy requirements . . . . .                 | 48        |
| A.6      | Temperature dependent model parameter regression . . . . .            | 50        |
|          | <b>List of Figures</b>  | <b>51</b> |
|          | <b>List of Tables</b>   | <b>52</b> |

# 1 Introduction and scope

## 1.1 Problem background

Global temperatures have been steadily rising at an unnatural pace not corresponding to normal geological processes since the advent of the industrial revolution [2], constituting the phenomenon which is broadly known as climate change. Some negative consequences of this include more extreme weather, considerable increase in the occurrence of natural climatological disasters, unprecedented sea level and acidity rise, loss of arable land and many more [3]. Decades of scientific research have linked this to increasing emissions of greenhouse gases (GHGs) [4], a group of gaseous compounds capable of absorbing and emitting radiant energy within the thermal infrared range. This category includes water vapor, carbon dioxide, methane, nitrous oxide, ozone and various fluorinated gases, among others [5]. These affect the radiative properties of the atmosphere making it reflect more sunlight towards the planetary surface, thus increasing overall temperatures in what is known as the greenhouse effect [4].

Climate change arises from anthropogenic greenhouse gas emissions, that is, by alterations of the chemical composition of the atmosphere caused by GHG-emitting human activities such as the burning of fossil fuels for energy generation [6]. Carbon dioxide or CO<sub>2</sub> is the most influential GHG. CO<sub>2</sub> atmospheric composition has unnaturally risen from 280 ppm in 1750 to the current all-time high of 416 ppm [7]. For comparison, a natural change of 100 ppm normally takes 5000 to 20000 years, while the recent increase of 100 ppm has taken just 70 years. Figure 1 shows the approximately linear relationship between anthropogenic CO<sub>2</sub> emissions and the global mean temperature increase in recent times. Climatological models predict a significant temperature increase if the atmospheric CO<sub>2</sub> concentration keeps on increasing at the current pace due to human emissions. International agreements like the recent one from Paris have been established as a combined effort to try to limit the temperature rise to 2°C by the year 2050[8].

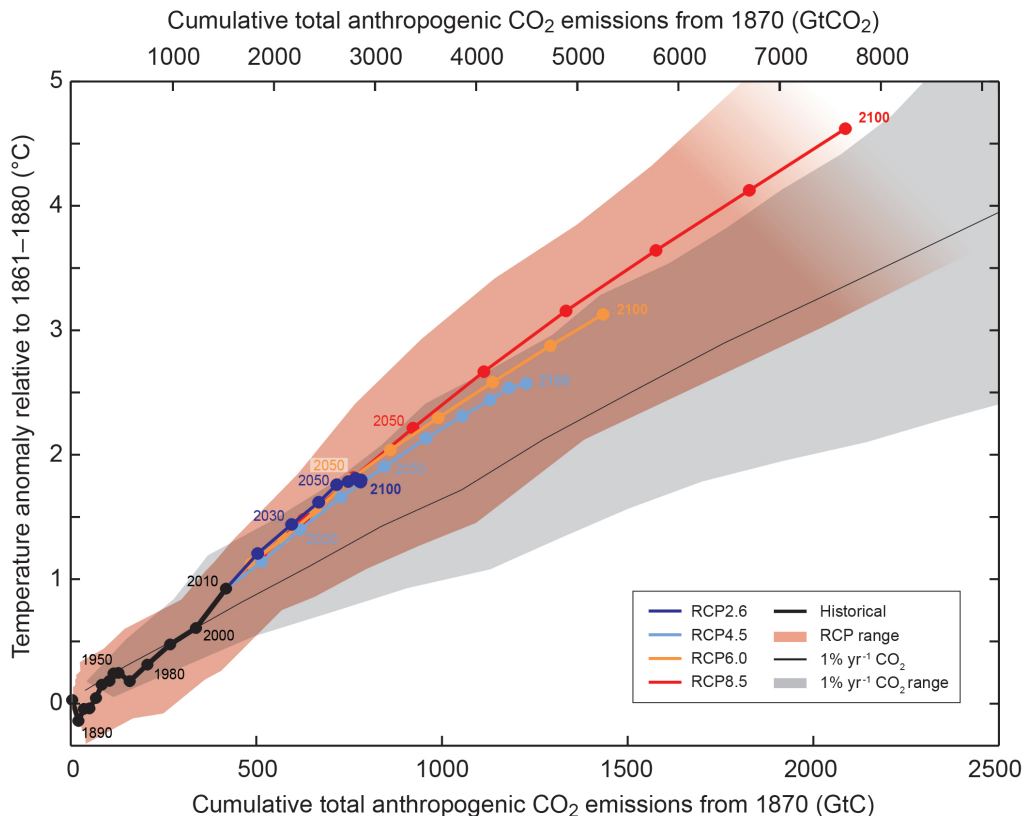


**Figure 1:** Global mean surface temperature increase as a function of cumulative total global CO<sub>2</sub> emissions, together with model predictions for different scenarios. For more information, see AR5 Climate Change: The Physical Science Basis [9].

There are multiple possible approaches to address climate change. Reduction of energy consumption does not seem likely to occur since it is required to maintain economic growth. Instead, it is on the rise and projected to increase significantly as developing countries become more industrialized [10]. On the one hand, research on

more sustainable energy sources has been ongoing for decades to find efficient, less polluting alternatives to fossil fuels [11]. On the other hand, there is research on Solar Radiation Management (SRM) climate engineering. It would affect the radiative properties of the atmosphere to reduce overall temperature without addressing CO<sub>2</sub> emissions, but the potential consequences of its application are still under research. Carbon Capture and Storage (CCS) is a complementary approach based on process technology to capture most of the CO<sub>2</sub> produced in large stationary sources such as fossil fuel based power plants. Subsequently, the CO<sub>2</sub> is stored in some manner (i.e. underground mines or ocean bottoms) to keep it outside the carbon cycle. A related approach is Carbon Capture and Utilization (CCU) which instead proposes the use of captured CO<sub>2</sub>, for example, as a chemical feedstock.

Current efforts have so far fell short on achieving a "carbon-neutral" or "net-zero" climate scenario, in which the atmospheric CO<sub>2</sub> concentration would be kept stable in a way similar to an unaltered carbon cycle. This would require total CO<sub>2</sub> emissions to be equal or lower than the amount of CO<sub>2</sub> that is removed naturally by carbon sinks. In order to address this, so-called Negative Emission Technologies (NETs) can be used to offset CO<sub>2</sub> emissions from diffuse CO<sub>2</sub> sources such as aviation, long-distance transport, and shipping [12]. This category includes the methods whose application results in an overall removal of CO<sub>2</sub> from the carbon cycle [13]. It is most important to take into account, however, that the approaches mentioned here are not exclusive from each other. Most likely, a better result can be reached by combining them to different degrees [6], as shown in Figure 2.

Most NETs are still in the research phase. So far, the only NET that has been demonstrated to work in a commercial scale is reforestation, but it alone would most likely not be enough to reach net-zero emissions due to the finite amount of fertile soil on the planet [14]. Biochar soil amendment, Bio-Energy coupled with CCS (BECCS), ocean fertilization and Direct Air Capture (DAC) are other approaches to negative emissions [13], of which the latter is the main topic of this work. DAC is defined as the direct separation of CO<sub>2</sub> from ambient air, producing a CO<sub>2</sub>-rich stream. It addresses the main shortcoming of conventional carbon capture because it can be used to capture CO<sub>2</sub> not only from point sources but also from distributed ones [15]. Considering that roughly half of the yearly anthropogenic CO<sub>2</sub> emissions come from these distributed sources, the advantage of NETs compared to regular carbon capture is clear. DAC has also a higher potential than most other NETs in terms of the amount of CO<sub>2</sub> that can be potentially removed [16, 17].

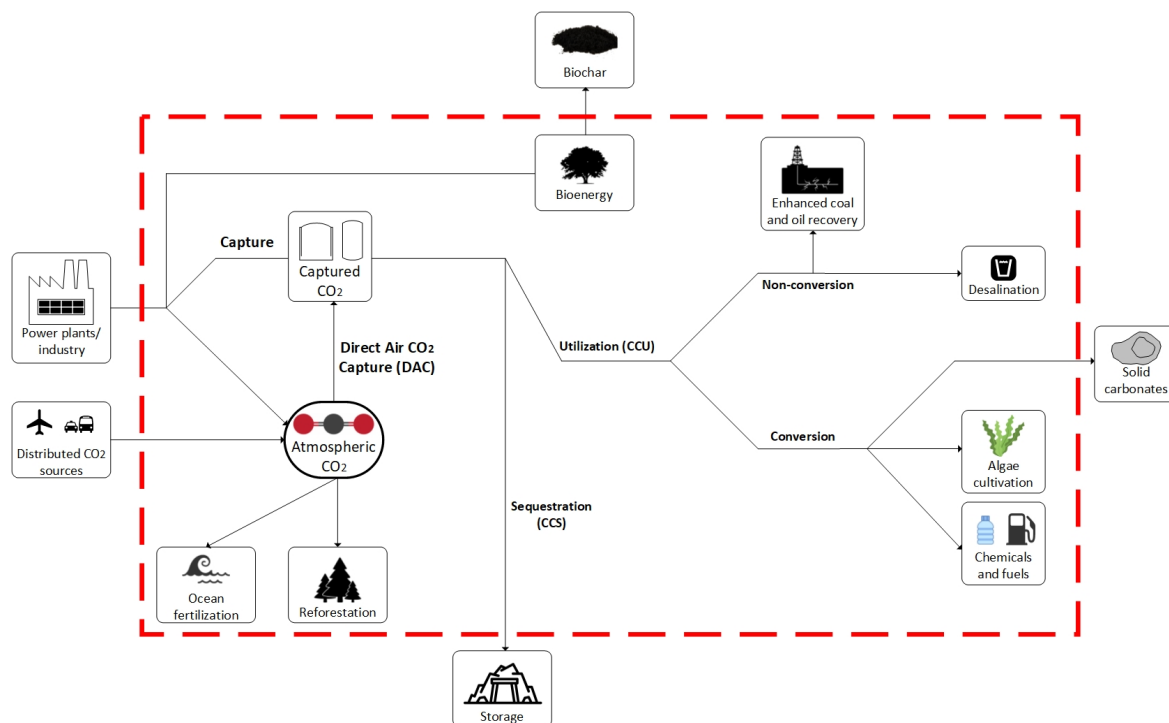


**Figure 2:** A selection of carbon capture pathways in relation to the carbon cycle. The dashed line represents the boundaries of the cycle at the relevant timescale.

## 1.2 Direct air capture of CO<sub>2</sub> on amine adsorbents

The most widely studied DAC methods are based on the use of sorbents which harness the potential of chemical affinity towards the molecule, due to the relatively low concentration of CO<sub>2</sub> in the atmosphere [15]. The first DAC method that was proposed is the use of calcium hydroxide adsorbents to react with atmospheric CO<sub>2</sub> forming calcium carbonate [18]. It has been studied for about two decades, and different processes are currently being developed like causticization, but there are significant drawbacks in this approach relating to its large energy demand and limited efficiency. The heat requirement per unit of CO<sub>2</sub> captured is expected to be similar to that of liquid amine adsorbents applied to flue gas (~130 kJ/mol), which is the benchmark process for the conventional carbon capture approach [15]. Other DAC methods that have been researched include electrochemical CO<sub>2</sub> scavenging, membrane technology, mineral carbonation and photocatalytic CO<sub>2</sub> conversion. Most of these are prohibitively energy-intensive or still in the research phase [15].

The use of solid adsorbents has also been extensively studied, such as inorganic alkali adsorbents similar to those used in the paper industry for causticization but in a solid form instead of in a solution. However, by far the use of solid-supported amine materials for DAC is the most reported research on the topic of DAC. These are composed of a support phase which can be organic or inorganic in nature and an active phase composed of primary, secondary and/or tertiary amines. Their use is based on a chemisorption reaction between CO<sub>2</sub> and the amines which allows for significant productivity even at low temperatures and concentrations [15].

The main advantages of amine sorbents compared to others for DAC are their higher CO<sub>2</sub> capacity and selectivity, faster uptake rates, lower heat capacity, and lower desorption energy requirement [19]. The last one is key, since a minimum of 1400 m<sup>3</sup> of air at normal conditions have to be processed to capture a kilogram of CO<sub>2</sub> (assuming 100% efficiency at 400 ppm concentration) [20]. This assortment of characteristics allows for a potentially lower energy demand in the process compared to most other sorbents.

A vast assortment of supported solid sorbents for CO<sub>2</sub> capture can be found in literature. In subsection A.1 a broad review of these was performed to identify a most propitious sorbent for use in the development of an adsorbent-based DAC process. In conclusion, the amine sorbent Lewatit VP OC 1065<sup>TM</sup> was selected due to its reasonably good CO<sub>2</sub> capacity at ambient conditions, fast uptake, adequate stability at regeneration conditions, high cyclic stability and scale-up feasibility due to its commercial availability. For the sake of brevity, in the rest of this work Lewatit VP OC 1065<sup>TM</sup> will generally be referred to simply as Lewatit, but it is not to be confused with the rest of the materials on the Lewatit product line.

## 1.3 Low temperature solid sorbent DAC process

Solid amine sorbents have the capability to be used in low temperature adsorption cycle processes. At the start of the two step cycle ambient air enters the unit containing the adsorbent bed, either naturally or with the help of fans. The CO<sub>2</sub> chemically binds to the sorbent and CO<sub>2</sub>-lean air leaves the system. Once the sorbent has reached the desired CO<sub>2</sub> saturation level, the desorption step takes place to regenerate the sorbent. The driving force of adsorption is reversed, causing the CO<sub>2</sub> to desorb. This can be done in different ways, the most common being Pressure Swing Adsorption (PSA) and Temperature Swing Adsorption (TSA).

A PSA process leverages the increased attraction to the sorbent that the adsorbate undertakes at higher pressures by performing the adsorption step at a higher partial pressure than the desorption step, whereas a TSA process uses temperature as a driving force by applying a temperature increase during the desorption step. For this type of cycle sorbent stability at desorption temperatures is then a key factor to account for. In practice it is necessary to have another mechanism present since the adsorbate needs to be removed from the unit after desorption has been carried out, be it via the use of a purge gas or a change in pressure. In the latter case, the process is a combination of both of these types of cycle known as a TPSA cycle [21].

As a result, a CO<sub>2</sub>-rich stream is produced. Once the amount of CO<sub>2</sub> bound to the sorbent has been reduced to the desired value, the adsorption step takes over again to restart the cycle. An example of such a cycle is shown in Figure 3. Depending on the sorbent and environmental conditions, some of the water naturally present in the air may also be adsorbed during the adsorption step. It will then have to be desorbed during regeneration, which increases the thermal energy requirements of the step. Pure CO<sub>2</sub> can be produced using a condensable purge gas such as steam.

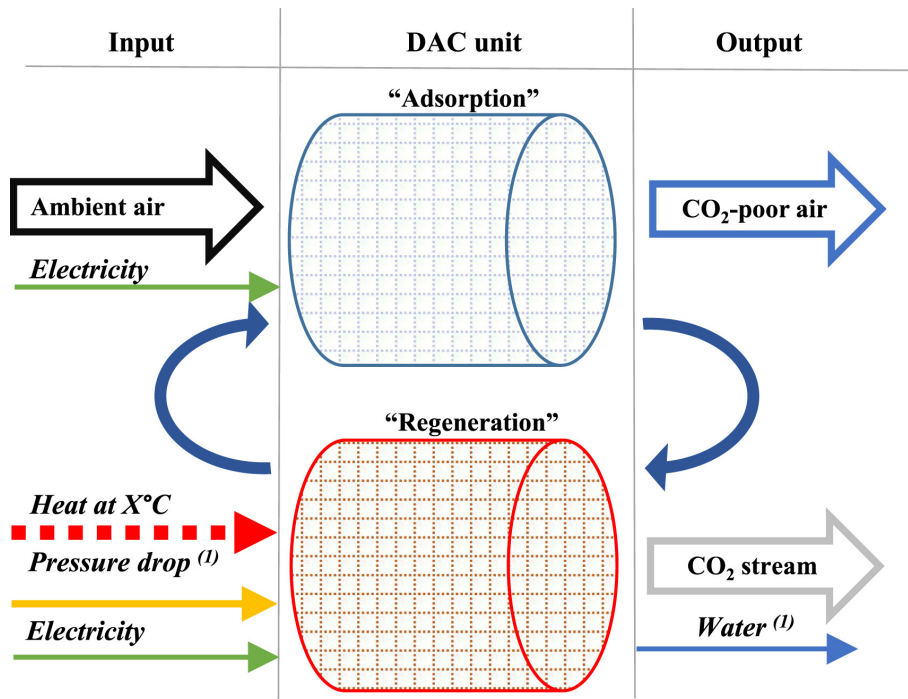


Figure 3: Example of a general low temperature solid sorbent DAC system [22]. (1) May not apply in some systems.

## 1.4 Problem definition

Despite its potential, DAC via amine adsorbents is a recent topic of research whose large-scale feasibility is still unproven. This means that key practical issues are still poorly addressed. The interaction between atmospheric water vapor, CO<sub>2</sub> and the sorbent is crucial for regeneration in DAC processes, since the presence of adsorbed water during desorption causes an additional "energy penalty" to arise [20]. On the other hand, the presence of water during the adsorption step increases the amount of CO<sub>2</sub> that can be adsorbed at equilibrium [1]. This creates a trade-off situation that requires more research to understand. CO<sub>2</sub> adsorption over Lewatit is well characterized in literature[23], but water adsorption is still very poorly understood as will be discussed in subsection 2.1.

## 1.5 Research goals

The main goal of this thesis is:

*Characterize the adsorption of water over Lewatit to contribute to the development of a future DAC process.*

The goal can be realized by answering the following two research questions, which themselves contain subgoals to put them into perspective:

1. *How can we gain a deeper understanding of water adsorption over Lewatit?*

- Establish a H<sub>2</sub>O adsorption capacity correlation with physical meaning as a function of the relative humidity of the air feed based on experimental results.
- Find out whether there is a temperature dependence of the water adsorption capacity within the relevant temperature range, and include it in the adsorption model if present.
- Study related phenomena, such as the monolayer adsorption behavior of water at lower values of relative humidity, and the possible hysteresis phenomenon.

2. *How can the results of this research be used for the conceptual design of an improved DAC adsorption-desorption cycle?*
- Minimize the water desorption energy penalty of the cycle per unit of CO<sub>2</sub> by analyzing the trade-off described in subsection 1.4.
  - Describe the impact that related adsorption phenomena such as hysteresis could have on the process.

## 2 Literature study

This section contains the information required to perform the experimental work and obtain results conducive to achieving the main goal. Mathematical models capable of representing the relevant phenomena taking place in the system are also described here and will be elaborated on in the following sections. Several other pieces of published information relevant to this research are discussed as well.

### 2.1 Water adsorption over Lewatit

Veneman et al. [1] performed equilibrium experiments for the water-Lewatit system, whose results are shown in Figure 4. Most of these results were obtained by varying temperature while keeping water concentration constant and as such cannot be used to study the isothermal behavior of the sorbent.

The adsorption behaviour of H<sub>2</sub>O on Lewatit shows the features of physical multilayer adsorption. The distinction is clearly reflected in the differences in adsorption heat ( $\Delta H_{ads,H_2O} = 43$  kJ/mol,  $\Delta H_{ads,CO_2} = 70 - 80$  kJ/mol) [1] and capacity. The latent heat of vaporization of water at similar conditions ( $\Delta H_{vap,H_2O} = 41$  kJ/mol) is very close to the adsorption heat, which points towards physisorption [24]. H<sub>2</sub>O adsorption capacities as high as 12.5 mol/kg have been measured, in comparison to 2.5 mol/kg for CO<sub>2</sub> [1]. This means that unlike for CO<sub>2</sub>, the maximum water capacity is much higher than the density of available amine sites (see subsection 3.1), again pointing to physical adsorption behavior.

Furthermore, the sorbent affinity to water originates primarily from the amine groups. The support was found to contribute approximately 15% of the total water capacity at 75% RH and had a negligible contribution at 33% RH [25].

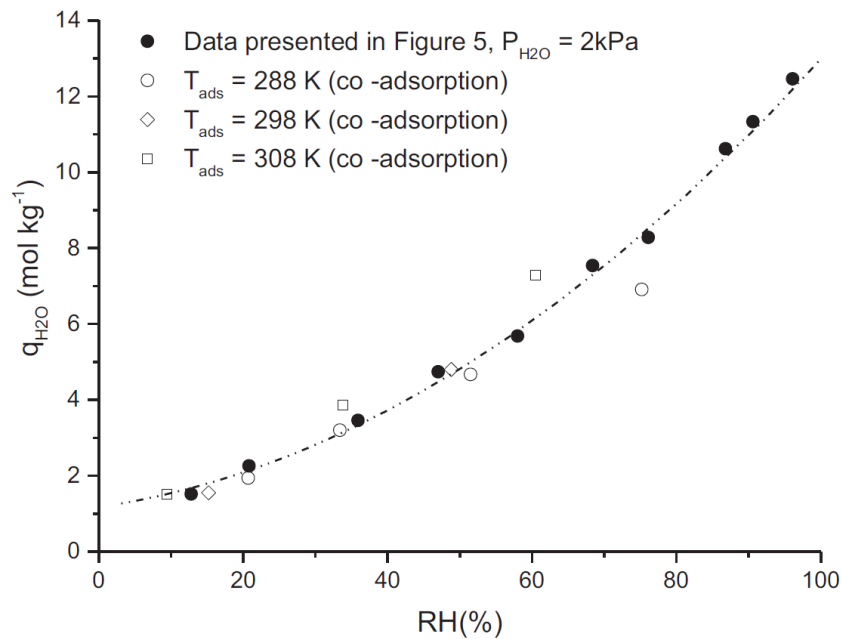


Figure 4: Experimental data of H<sub>2</sub>O equilibrium capacities for Lewatit, without (black symbols) and with (white symbols) CO<sub>2</sub> present, at varying relative humidity [1].

### 2.2 Adsorption isotherm

A simple mathematical description of the adsorption phenomena taking place on the sorbent is necessary for the design of a process. Note that the expressions in this section are given for ideal mixtures, so partial pressures are used instead of adsorbate activities.

### 2.2.1 Isotherm classification

The adsorption isotherm classification of Aranovich-Donohue [26] proposes five different types of isotherm shape. Type I represents adsorption in microporous adsorbents. Type II and III isotherms are for macroporous adsorbents with strong and weak affinities, respectively. These materials present significant physisorption. Type IV and V isotherms are for mesoporous adsorbents with strong and weak affinities, respectively. Since Lewatit is a mesoporous sorbent, a representation of these two can be found in Figure 5a and Figure 5b. Water adsorption over Lewatit proceeds mainly through physisorption, which means that the affinity towards water is weak. Thus, a Type V isotherm behavior is to be expected from the data.

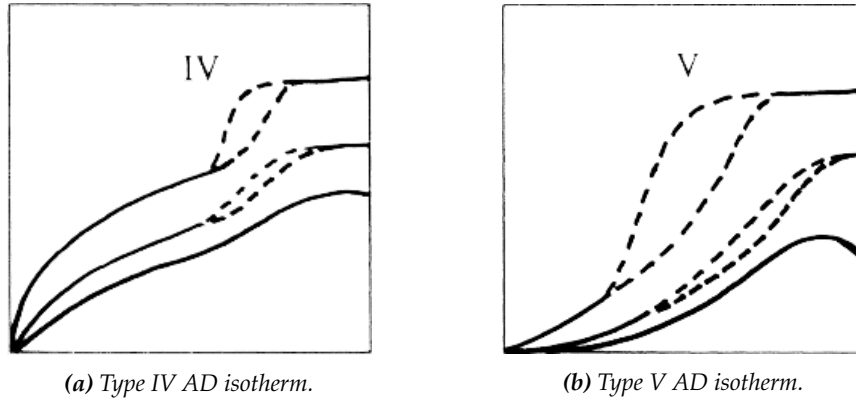


**Figure 5:** Isotherm types for mesoporous adsorbents. The curves represent adsorption capacity (Y axis) versus adsorbate activity (X axis).

### 2.2.2 Water isotherm model

In order to obtain a working isotherm model for H<sub>2</sub>O adsorption on Lewatit over a wide range of adsorbate pressures, three phenomena must be accounted for: the formation of the monolayer at low pressure of adsorbate, the consecutive formation of the multilayer and the effect of capillary condensation at higher partial pressures of adsorbate. The monolayer behavior is easy to account for by choosing an adsorption model that at low pressure reduces to the Langmuir isotherm. The prediction of multilayer behavior requires the model to have a built-in capability to account for the presence of successive adsorbate layers on top of each other. The capillary condensation refers to the point in which Van der Waals forces reach a value high enough to cause adsorbate condensation in confined pore spaces, causing them to fill with liquid adsorbate. This occurs because the saturation pressure in these spaces is lower than in a flat surface at similar conditions [24]. This behavior is complex and usually accounted for in an empirical manner.

The Langmuir model (Equation 1) is a simple, theoretical isotherm model which accounts for the surface coverage by balancing the relative rates of adsorption and desorption.  $b$  is the adsorption equilibrium constant related to the adsorption energy of the system, while  $q_m$  represents the monolayer capacity. It is generally preferred due to its theoretical significance, but it can only account for monolayer formation [24]. The Brunauer-Emmet-Teller (BET) model (Equation 2) is an extension of the Langmuir isotherm commonly used due to its capacity to account for both monolayer and multilayer formation. This model is recommended by the IUPAC for characterization of adsorption on porous solids, and thus useful as a reference [27].

$$\text{Langmuir} : \frac{q}{q_m} = \frac{bp}{(1 + bp)} \quad (1)$$

$$\text{BET} : \frac{q}{q_m} = \frac{C \cdot p/P^{sat}}{(1 - p/P^{sat}) \cdot (1 + (C - 1) \cdot p/P^{sat})} \quad (2)$$

The parameter  $C$  is related to differences of free enthalpy between the two adsorbate states of monolayer and multilayer (which BET assumes equivalent to the liquid state in terms of enthalpy) [28]. The larger it is, the higher the energy of the molecules in the monolayer is compared to those in subsequent layers. When  $C = 1$ , both states would have the same energy.

In most water adsorption data, three different sorption stages may appear throughout the range of adsorbate activity from 0 to 1. Sorption stage 1: micropores (if there are any) get filled, and the monolayer forms. Stage 2: Subsequent layers start appearing, at some point capillary condensation starts occurring. Stage 3: liquid-like interactions take over, pore condensation is the main phenomenon from this point on [28]. BET is valid in the pressure range of  $p/P_0=0.05-0.3$ ; for relative pressures above 0.3, the presence of capillary condensation is practically guaranteed. This makes BET lose its predictive power along the second sorption stage. Mesoporous materials, a category that includes Lewatit, are typically filled in the region of capillary condensation ( $p/P_0 > 0.3$ ) [24], which means BET will most likely not be adequate.

To account for a larger range of pressures, various other models have been developed. Guggenheim, Anderson and de Boer developed the GAB isotherm, which serves as an extension of BET valid for higher relative pressures ( $p/P^{sat} \leq 0.85$ ) [27]. Its expression is shown in Equation 3. This model considers the sorption state of adsorbed molecules to be identical throughout the multilayer but different from that of the pure liquid. The parameter  $k$  was thus introduced to account for the difference in free energy between these two states [28]. In BET,  $k = 1$ , which means that the adsorbate enthalpy in the multilayer is identical to that of the liquid state, but in GAB  $k \in [0, 1]$ .  $k$  can also be described as an approximation of how much higher the vapor pressure is in the GAB multilayer ( $p_{GL}$ ) compared to the pure liquid ( $p_{sat}$ ), as in  $k \approx p_{sat}/p_{GL} < 1$  [28]. Due to the mathematical properties of the models, the value of  $q_m$  obtained from GAB is always higher than from BET, and the opposite is true for  $C$ .

$$GAB : \frac{q}{q_m} = \frac{C \cdot k \cdot p/P^{sat}}{(1 - k \cdot p/P^{sat}) \cdot (1 + (C - 1) \cdot k \cdot p/P^{sat})} \quad (3)$$

Timmermann [28] suggests that unless the value of  $k$  is experimentally confirmed to be nearly 1, the values of a GAB fit should be used instead of BET for the description of the system in physical terms. However, GAB is not perfect either. The GAB model implies an average enthalpy for all molecules adsorbed in the multilayer (implied in the fact that  $k$  is a single value), while in reality each subsequent layer has a lower enthalpy level than the previous one. The reason why GAB works within most of the capillary condensation range even though it does not explicitly include capillary condensation into the model is because the reduction of enthalpy of subsequent layers forming in the multilayer is compensated by the increase in enthalpy due to liquid-like interactions (which are not taken into account in the model). In the third sorption stage these take over and most molecules from then on are in a liquid-like state, making GAB lose more of its predictive power the further it goes into that region [28].

The change of adsorption capacity with temperature can be accounted for by introducing a temperature dependency in parameters  $q_m$ ,  $C$  and  $k$ , as shown in Equations (4) to (5). Both  $C$  and  $k$  are expected to change with temperature owing to their thermodynamic nature. Theoretically  $q_m$  is a measure of the capacity of the monolayer and thus should only depend on the number of available active sites. However, some authors propose that it can be affected as a result of physical or chemical changes of the sorbent induced by temperature [29].

$$C = C_0 \cdot \exp\left(\frac{\Delta H_C}{RT}\right) \quad (4)$$

$$k = k_0 \cdot \exp\left(\frac{\Delta H_k}{RT}\right) \quad (5)$$

$$q_m = q_{m,0} \cdot \exp\left(\frac{\beta}{T}\right) \quad (6)$$

$\Delta H_C = H_{mono} - H_{multi}$  represents the difference in enthalpy between monolayer and multilayer adsorption. Due to the exothermic nature of the interaction between water and the primary adsorption sites it is expected to be positive.  $\Delta H_k = H_{liq} - H_{multi}$  represents the difference between the heat of vaporization of the adsorbate and the heat of adsorption on the multilayer. This value is negative since molecules in the multilayer are more loosely bound to each other in the multilayer state than in the liquid state. However, a positive value can be sometimes obtained in cases such as adsorption coupled with the endothermic dissolution of fruit sugars [29]. Figure 6 shows these enthalpic parameters in context.  $\Delta H_{is}$  refers to the isosteric adsorption heat, while  $\Delta H_v$  is the heat of vaporization.  $\Delta H_{is}$  can be obtained from the fit parameters according to Equation 7.

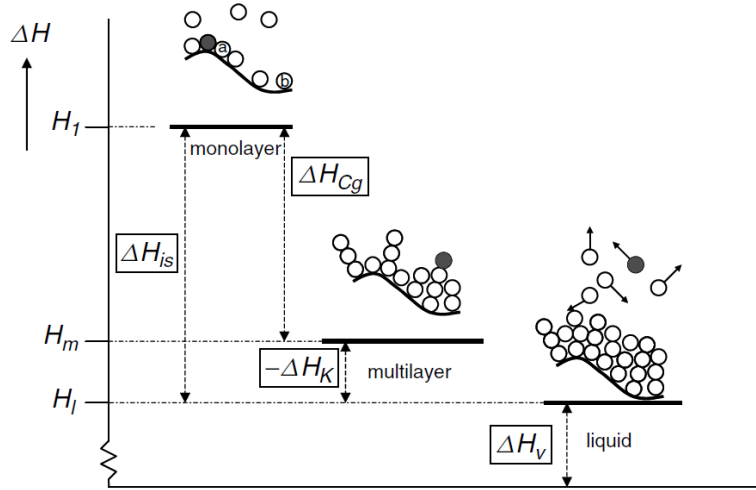


Figure 6: Enthalpy of water molecules (shaded) at different energy levels represented by GAB enthalpic parameters [29].

$$\Delta H_{is} = \Delta H_C + (-\Delta H_k) \quad (7)$$

The heat of adsorption of the adsorbate ( $\Delta H_{ads,w}$ ) is of capital importance for process design, since it is necessary to calculate the energy requirements of desorption. At constant capacity, the difference between the temperature and the partial pressure of water can be used to calculate  $\Delta H_{ads,w}$  by using the Clausius-Clapeyron relation as described in Equation 8.

$$\Delta H_{ads} = R \frac{\ln(p_2/p_1)}{\frac{1}{T_1} - \frac{1}{T_2}} \quad (8)$$

The degree of monolayer occupation ( $\xi$ ) can be estimated for a given adsorbate activity using the values of parameters  $C$  and  $k$  according to Equation 9. While the BET model assumes complete surface coverage, the GAB model implies incomplete coverage due to adsorbate molecules "jamming" at the surface. This means that the BET model necessarily implies  $\xi_{max} = 1$  while for GAB it is the case that  $\xi_{max} < 1$  [30].

$$\xi = \frac{C \cdot k \cdot p / P^{sat}}{1 + (C - 1) \cdot k \cdot p / P^{sat}} \quad (9)$$

To account for limiting cases near saturation pressure, Aranovich developed another modification of the BET isotherm[31]. The BET model assumes equal heats of adsorption for any number of layers, while the Aranovich model assigns a different value to this variable for a molecule depending on the number of layers. Mathematically, the main difference between the two is in the exponent of the term  $(1 - p/P^{sat})$  in the denominator of both equations. For BET the value is one, while for Aranovich it is one half. The Aranovich isotherm expression is shown in Equation 10.

$$\text{Aranovich: } \frac{q}{q_m} = \frac{b \cdot p / P^{sat}}{(1 - p / P^{sat})^{1/2} \cdot (1 + b \cdot p / P^{sat})} \quad (10)$$

Various modifications of the Aranovich isotherm have been proposed to fit experimental data. Aranovich and Donohue proposed its use as a modular equation, hereby called the AD isotherm, using it together with other isotherm models with different properties. The base of the model is Equation 11, which is used to describe the divergence of adsorption capacity under pressures near saturation depending on parameter  $d$ . This is an empirical value, in contrast with Equation 10 where it was fixed as one half. Introducing this divergence allows this model to obtain a better fit compared to the GAB model in this part of the activity range in which liquid-like interactions take over. According to the authors, the value of the exponent must be within  $d \in [0, 1]$  [31]. The  $f(P)$  term corresponds to the secondary isotherm model used to model the behavior at the lower ranges. Examples of

different possibilities for this are shown in Equations (12) to (13). They are expected to be useful for pressures up to  $(p/P^{sat} \leq 0.95)$  [32].

$$AD : q = \frac{f(p)}{(1 - p/P^{sat})^d} \quad (11)$$

$$Langmuir : f(p) = \frac{q_m b p}{(1 + b p)} \quad (12)$$

$$Sips : f(p) = \frac{q_m (b p)^{1/n}}{1 + (b p)^{1/n}} \quad (13)$$

$$Toth : f(p) = \frac{q_m b p}{(1 + (b p)^{t_h})^{1/t_h}} \quad (14)$$

Both Sips and Toth isotherms are empirical modifications of the Langmuir isotherm [33]. The Sips isotherm is a combination of Langmuir and the empirical Freundlich isotherm, which approaches Langmuir at low values of adsorbate concentration and Freundlich at higher values. This makes it capable of dealing with surface heterogeneity. The Toth isotherm reduces to the Langmuir isotherm at  $t_h = 1$ . This parameter  $t_h$  thus characterizes the heterogeneity of the adsorption system. If  $t_h > 1$ , the system is said to be heterogeneous [33]. It correctly predicts both the Henry law limit and the finite saturation limit [24], which means that in the lowest range of concentration it predicts a linear behavior of capacity with adsorbate pressure, and at higher values it predicts the formation of a finite amount of multilayers.

### 2.3 Adsorption hysteresis

Adsorption hysteresis is a phenomenon typically observed in mesoporous sorbents. In materials that present it, the equilibrium capacity for the same value of temperature and concentration changes whether it is approached by adsorption (forwards) or by desorption (backwards). This phenomenon is generally associated to the filling and emptying of the pores. When going forwards, condensation occurs near the pore walls, and at some point the pore is filled with condensed adsorbate. When going backwards on the hysteresis loop, the adsorbate evaporates from the liquid meniscus with a given angle. Eventually the condensed adsorbate reaches a meta-stable state at a higher equilibrium capacity [34]. This is shown graphically in Figure 7. The classification of the different types of hysteresis loops is represented in Figure 8.

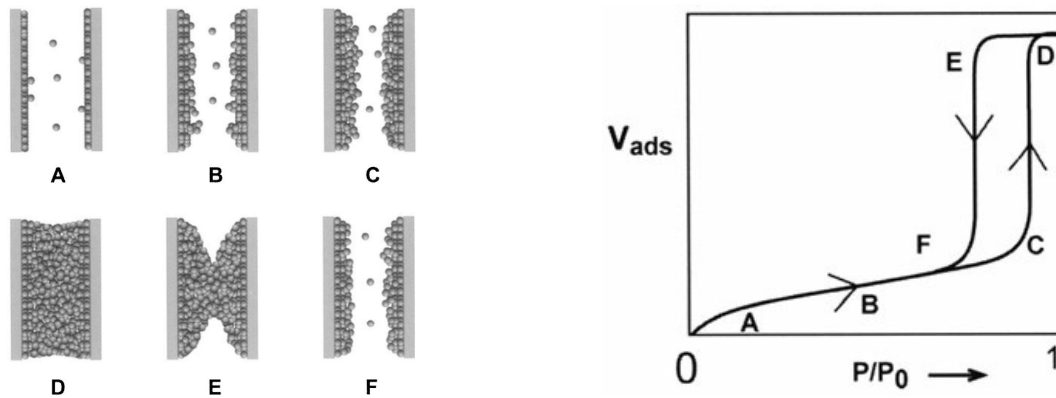
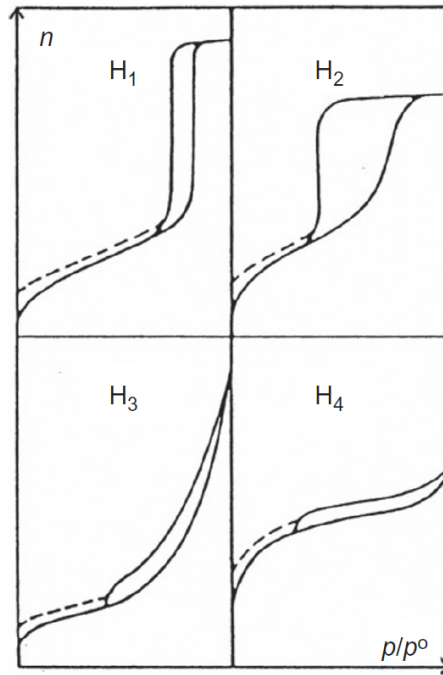


Figure 7: Graphical description of the hysteresis mechanism of pore filling [35].



**Figure 8:** IUPAC classification of hysteresis loops[34].

The pore radius at which pore condensation takes place for a given value of adsorbate activity is known as the Kelvin radius and can be calculated according to the Kelvin equation (Equation (15))[24].

$$r_K = \begin{cases} \frac{V_M \sigma}{RT \ln(P_0/P)} & (\text{Adsorption}) \\ \frac{2V_M \sigma \cos \theta}{RT \ln(P_0/P)} & (\text{Desorption}) \end{cases} \quad (15)$$

### 3 Materials and methods

The adsorbent material used in the adsorption-regeneration experiments is Lewatit VP OC 1065<sup>TM</sup> bought from Lanxess, which is described in depth on this section. Simulated air is used as feed and produced by combining different quantities of N<sub>2</sub> and H<sub>2</sub>O. The two different experimental methods used in this work are described. One of them is based on the breakthrough curve of water in the outlet of the adsorption setup, the other in the weight difference before and after the adsorption equilibrium is reached.

#### 3.1 Lewatit VP OC 1065

Lewatit is a commercial amine-functionalized Anion Exchange Resin (AER) meso-porous adsorbent. Structurally, it is a benzylamine cross-linked polymer based on a polystyrene (PS) and divinyl benzene (DVB) backbone [25, 1, 36]. Its molecular level structure is shown below, with the polymeric PS-DVB backbone in Figure 9 and the different constituent monomers in Figure 10. Its properties are shown in Table 1.

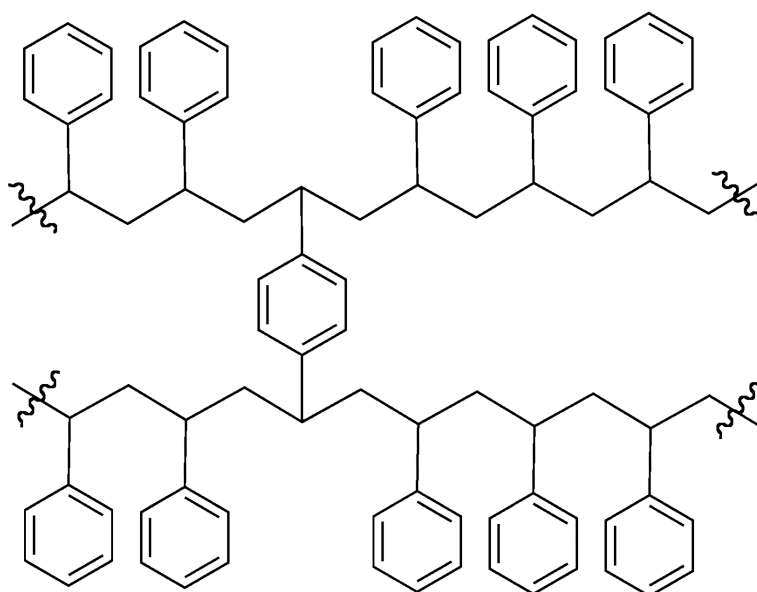
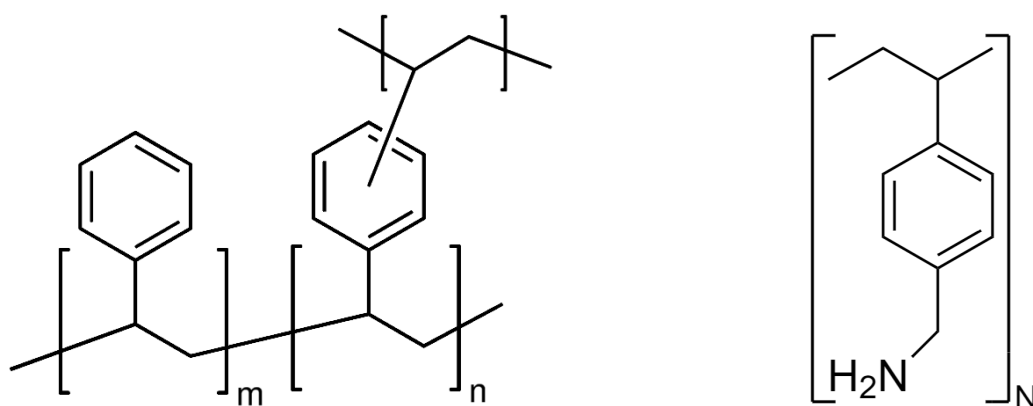


Figure 9: Representation of a fragment of the PS-DVB polymer backbone of Lewatit VP OC 1065<sup>TM</sup>.



(a) Backbone monomers. "m" represents a styrene monomer while "n" represents the DVB cross-linking with other ramifications.

(b) p-vinylbenzylamine monomer.

Figure 10: Constituent monomers of Lewatit VP OC 1065<sup>TM</sup>.

**Table 1:** Physical and chemical properties of Lewatit.

|  |                          |      |
|--|--------------------------|------|
| Physical appearance                                | Opaque yellow beads      | [36] |
| Matrix   | Cross-linked polystyrene | [36] |
| Functional group                                   | Primary amine            | [36] |
| Total exchange capacity (min Eq/L wet resin)       | 2.2                      | [36] |
| Bulk density ( $\pm 5\%$ g/L)                      | 630–710                  | [36] |
| Stability temperature range ( $^{\circ}\text{C}$ ) | $20 \pm 100$             | [36] |
| Effective size (mm)                                | 0.47–0.57                | [36] |
| Water retention (wt%)                              | 65–70                    | [36] |
| Approximate pore volume (cm <sup>3</sup> /g)       | 0.37                     | [37] |
| Average pore diameter (nm)                         | 38.5                     | [37] |

Lewatit has a reasonably high CO<sub>2</sub> adsorption capacity. The maximum theoretical amine loading measured by elemental analysis, after accounting for the cross-linking, is approximately 6.7 mol amine/kg dry resin [38]. This is roughly twice that of the minimum 3.5 equivalents/kg dry resin determined by the manufacturer through titration, which implies that part of the amines are unavailable for reaction, for example by being buried in bulk polymer. For this reason, the CO<sub>2</sub> capacity was determined via other experimental methods. The maximum theoretical capacity of 3.37 mol CO<sub>2</sub>/kg was measured using energy-dispersive X-ray spectroscopy (EDS), while the maximum capacity reported in adsorption experiments was 2.5 mol CO<sub>2</sub>/kg. There could be several reasons for this difference between the expected and actual capacity such as small pores being inaccessible, or the use of partial pressures of 1 atm of CO<sub>2</sub> or lower [39]. Mass transfer resistances present in the available range of operational temperature could also have accounted for this, but they were found to be insignificant [23].

Cyclic stability studies have shown that, in order to prevent thermal degradation, regeneration of Lewatit should be carried out at temperatures lower than 150  $^{\circ}\text{C}$ , and also in the absence of oxygen for temperatures above 70  $^{\circ}\text{C}$ . At high partial pressures of CO<sub>2</sub> (close to 1 bar) the temperature should not exceed 120  $^{\circ}\text{C}$  to avoid extensive urea formation [38]. Steam stripping has been proposed as a regeneration method due to increased sorbent stability and capacity, making it seem more promising than the more expensive nitrogen regeneration [38, 20]. Cyclic stability of Lewatit has been demonstrated for up to 280 cycles for a nearly pure CO<sub>2</sub> feed [40].

### 3.2 Breakthrough method

The setup present at the Meander laboratory is shown in Figure 11, and was used in the first set of water equilibrium experiments, from now on referred to as the "Breakthrough method" experiments. It consists of a N<sub>2</sub> gas supply, a gas humidifier comprised of two bubble columns to introduce water vapor in the feed and a temperature controlled reactor vessel that contains a fixed bed of adsorbent material inside of it. The relative humidity of the gas feed is measured using humidity sensors [B+B Sensors 0141 0316-224] in both inlet and outlet of the reactor vessel. High purity (Grade 5.0) N<sub>2</sub> was used in the experiments and the flow rates were controlled with Brooks mass flow controllers (SLA 5850 series), which allow us to produce gas streams with the desired flowrate and fractions of nitrogen and water.

The setup can be operated at different temperatures, using a water bath (Julabo F32/F25) or electrical heating (600W heat tracing controlled by Eurotherm 2132). Electrical heat tracing is also present in both inlet and outlet of the reactor and the humidifier outlet to prevent condensation when needed. The fixed bed reactor vessel has a diameter of 13 mm and a length of 600 mm. The temperature is measured by K-type thermocouples in the axial and radial center of the bed, outside the reactor wall and in both inlet and outlet. Pressure sensors are located in reactor inlet and outlet to detect possible pressure buildup and obtain more precise values of water concentration in the gas.

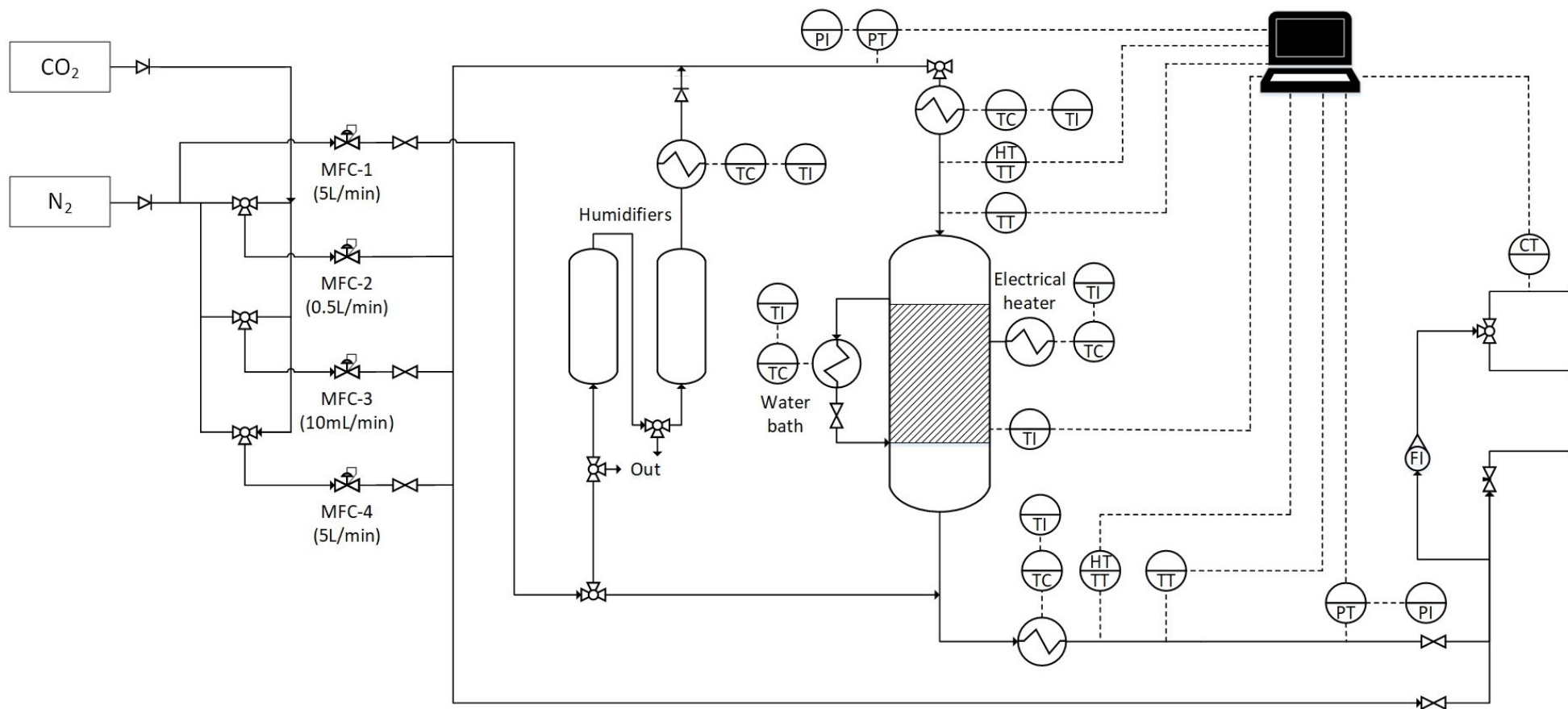
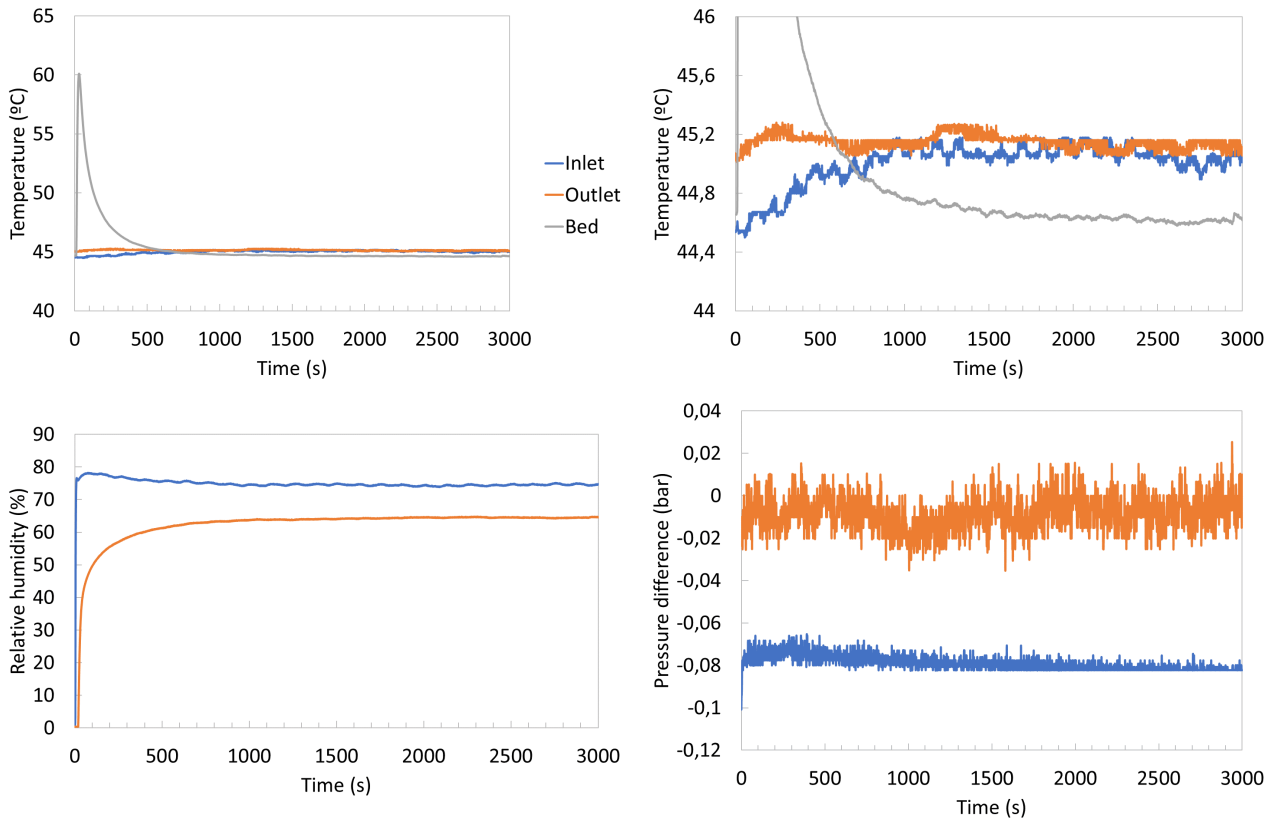


Figure 11: Process flow diagram of the adsorption-desorption setup.

Previous to the experiments, the Lewatit is completely desorbed by increasing bed temperature to 80°C and feeding nitrogen through the bed. During the experiment, nitrogen is fed to the humidifiers and the resultant N<sub>2</sub>/H<sub>2</sub>O mixture is mixed with N<sub>2</sub> to obtain the desired value of RH and sent to the reactor vessel. The sensors register one data point per second for each magnitude out of the seven that are being measured. Temperature, pressure difference and relative humidity are being measured in both inlet and outlet, as well as the temperature on the sorbent bed. By using these data, we obtain the breakthrough curves of the water which are later used to obtain the adsorbed water capacity based on the unit mass balance. An example of the data obtained from the setup can be found in Figure 12. Note the temperature spike in the bed at the beginning of the experiment, caused by the energy released by water adsorption.

Experimentally it was found that the position of the sensors inside the gas line affects the value measured in a way that can cause significant differences in the calculated equilibrium capacity. This was found to not be an effect of a laminar flow profile, since reducing the pipe diameter for increased turbulence did not improve the result. The issue could be caused by the presence of a dead zone in the upper part of the measuring line. For consistency, the sensors are always positioned at the same height and as close as possible to the bottom of the line, but without touching the steel pipe.



**Figure 12:** Data sample from a breakthrough method experiment. Note: the legend in the first graph applies to all graphs in the figure.

There are several steps to convert the data sets, which contain up to hundreds of thousands of data points, into a single datum of equilibrium adsorption capacity versus relative humidity. For each data point the saturation pressure of inlet, outlet and bed is calculated using the Arden-Buck equation (Equation 16), which is both precise and simple to use [41]. The value is then used to convert the relative humidity into the water mole fraction as shown in Equation 17. In it, the value of total pressure is obtained from the differential pressure measurements.

$$P_i^{sat} = 0.61121 \cdot \exp\left(\frac{18.678 - T_i}{234.5} \cdot \frac{T_i}{257.14 + T_i}\right) \quad (16)$$

$$X^W = \frac{RH \cdot P^{sat}}{P} \quad (17)$$

Using the known inlet flowrate and the calculated mole fraction of water, the water flowrate entering the bed can be calculated using Equation 18. Since the temperature of the bed is usually different than that of the inlet, the actual value of relative humidity in the bed will also differ and has to be obtained via Equation 19.

$$N_{in}^W = N_{in} \cdot \frac{X_{in}^W}{1 - X_{in}^W} \quad (18)$$

$$RH_{bed} = RH_{in} \cdot \frac{P_{in}^{sat}}{P_{bed}^{sat}} \quad (19)$$

The amount of adsorbed material can be calculated by combining the overall mass balance with the component mass balances of water and CO<sub>2</sub> (if present), resulting in Equation 20. The outlet flowrate is then obtained by the difference with the inlet as in Equation 21. If necessary, this allows us to calculate the adsorbed amount of each compound according to Equation 22. Finally, the value of equilibrium water adsorption capacity is obtained by adding up the amount of water adsorbed over the whole experiment time divided by the amount of sorbent material used, as shown in Equation 23.

$$N_{ads} = \frac{N_{in}^W - N_{in} \cdot X_{out}^W}{1 - X_{out}^W} \quad (20)$$

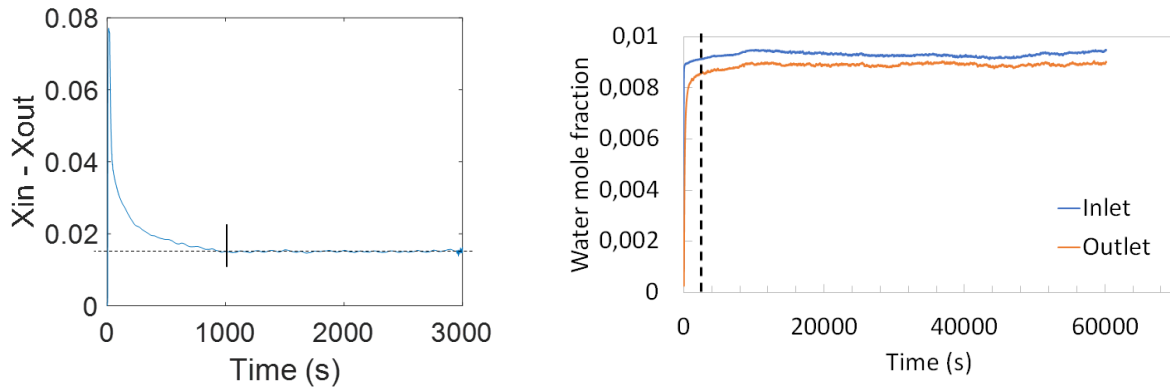
$$N_{out} = N_{in} - N_{ads} \quad (21)$$

$$N_{ads}^i = N_{in}^i - N_{out}^i \quad (22)$$

$$q_{eq}^i = \frac{\sum_{t=1}^{t=t_{equilibrium}} N_{ads}^i}{m_{sorbent}} \quad (23)$$

The experiment is run for a time long enough to reach equilibrium. The equilibrium point is obtained by studying the graph of the difference in concentration between inlet and outlet over time and finding the exact moment at which the value stops going down and stays relatively constant, as shown in Figure 13a. Once this is known the value of the adsorption capacity and bed humidity at that point constitutes the result of the experiment.

In practice it was found that this is further complicated by the use of two sensors, which require slightly different calibration. This creates a gap between the inlet and outlet water concentration, which is present long after equilibrium has been reached. Its value is nearly constant, depends on both the RH and temperature of the gas, and varies slightly due to random temperature and humidity fluctuations during the experiment (see Figure 13b). This causes the calculated value of adsorption capacity over time to keep on increasing (or decreasing) in a linear manner even after equilibrium.



(a) Difference between inlet and outlet water mole fraction capacity over time and identification of equilibrium point.

(b) Mole fraction over time for a different example experiment left for a long time.

**Figure 13:** Determination of equilibrium point for the breakthrough method. Note: the examples in Figure 13a and Figure 13b are given for two different experiments.

A way to correct for this mathematically was applied. The procedure is based on calculating the slope of the adsorption capacity over time after equilibrium, and then subtracting that constant value to the entire capacity dataset, as shown in Figure 14.

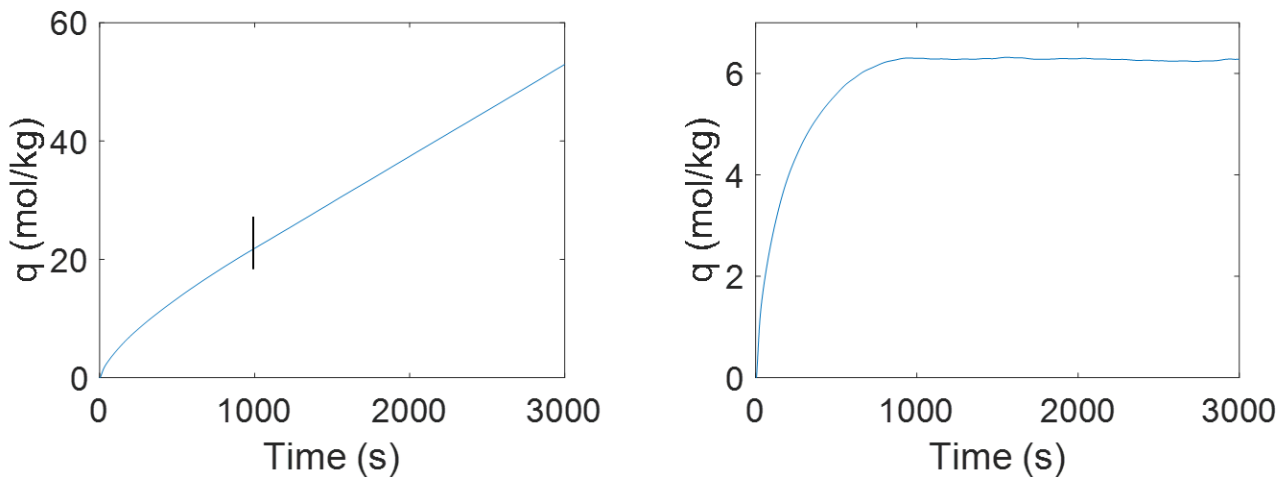


**Figure 14:** Water adsorption capacity over time before and after correction for the concentration gap.

Two different type of breakthrough experiments were performed: "single" experiments in which the bed was regenerated after equilibrium had been reached, and "multiple" experiments in which once equilibrium was established the RH or temperature of the feed gas was changed. The use of multiple experiments allows to obtain values of equilibrium capacity going from a high RH equilibrium to a low RH one, thus allowing to study the hysteresis behavior of the material. The two types of experiments were shown to be in good accordance with each other, as replications showed. A side by side comparison can be seen in Figure 15.

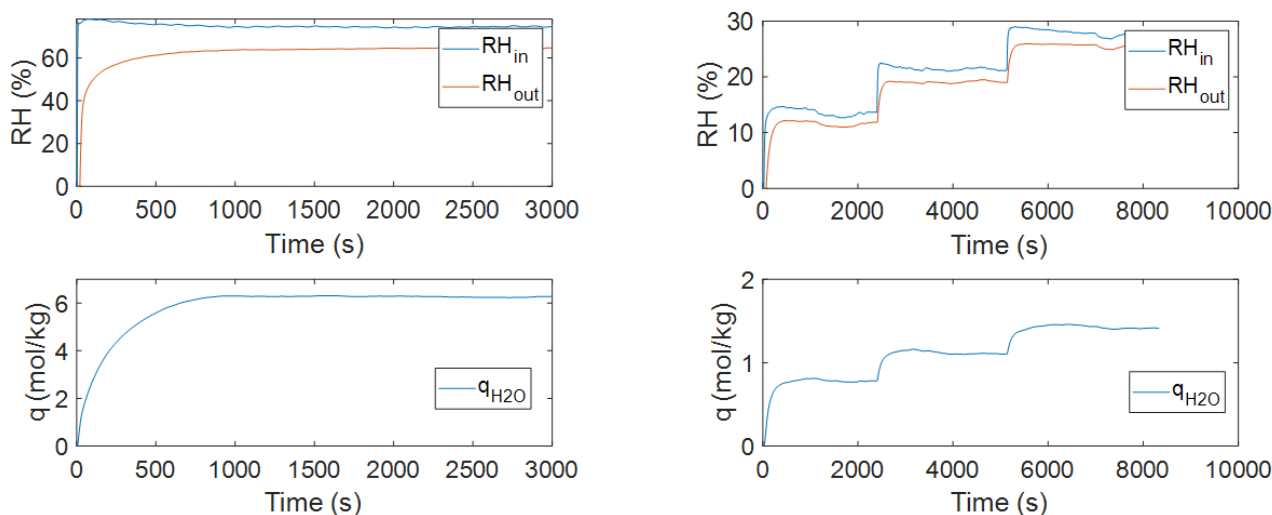


**Figure 15:** Examples of raw RH data and calculated capacity over time for single (left) and multiple (right) water breakthrough experiments.

The measurement of water adsorption capacity at low values of bed humidity is challenging. The humidity sensors are limited by the minimum value of RH they can measure. Below 20% relative humidity the systematic error of the measurement increases from  $\pm 2\%RH$  to a value that could be much higher than the measurement value. They also had a minimum measurement threshold at around  $RH = 5\%$ , under which no relative humidity was measured even though the gas contains water.

In order to bypass this, it was decided to measure a broad humidity range at a bed temperature higher than ambient ( $T_{bed} = 45^\circ C$ ). This allows to measure the humidity of the feed at ambient temperature, while the humidity in the bed is actually lower due to the increased temperature. For reference, measuring  $RH = 20\%$  at ambient temperature approximately equates to  $RH = 5\%$  at  $45^\circ C$ . Unfortunately, high RH values cannot be directly measured at the higher bed temperature, since a fully saturated feed at ambient temperature is equal to a bed humidity of  $RH_{bed} = 27\%$ . To solve this a water bath was connected to the bubble columns so that the gas becomes saturated at a higher temperature. An additional heat tracing had to be installed between the humidifier and the piping to prevent condensation, together with a Teflon tube to withstand high temperatures.

In summary, the high temperature experiments below 20% RH were performed by measuring RH at ambient temperature, while RH values above 20% were reached by increasing the temperature at which the gas was humidified and measured.

### 3.3 Gravimetric method

The second set of water equilibrium measurements was obtained in a simplified version of the laboratory setup. The reactor vessel in Figure 11 is substituted by a small flask containing the sorbent as shown in Figure 16. This method was developed during this study to overcome the shortcomings of the breakthrough method, as will be discussed in subsequent chapters. Before the experiment, a sorbent mass of approximately 1 gram is put in the flask, and is then left inside the vacuum oven for several hours at  $90^\circ C$  to remove all adsorbed water. The small amount of sorbent over the glass surface ensures total contact of the bed with the gas inside the flask. To start the experiment, the flask is capped to prevent adsorption from the environment and cooled down to the experimental temperature before measuring the weight, ideally while flowing pure  $N_2$  through the bed. This weight measurement will be considered as the "blank" mass for the experiment. This was found to be a key step because at a temperature different than the experimental one the weight of the empty flask measured in the precision scale is significantly different, resulting in an unsteady reading. This phenomenon could also be replicated at temperatures lower than ambient. Some possible causes could be expansion/contraction of metal parts in the scale, change in density of the glass or gas, or water adsorption on the glass surface.

The water bath was used for the experiment sets that were performed at a temperature different than ambient. In this case, the blank measurement was obtained by measuring the weight of the dried, sorbent-containing flask after a certain amount of time in the bath in a pure  $N_2$  atmosphere. The reason is that the weight of the setup was found to change after being exposed to the water bath for several hours, even when the temperature stayed

constant. This is most likely caused by water adsorption in the glass. Once the weight measurement of the setup is constant over at least one hour, the experiment can be started. The difference in weight measured will then only be caused by the adsorbed water in the bed. If this procedure is not done right, based on the amounts of sorbent used on the bed (around 1 gram) this could mean an error of over 100% on the capacity result at low values of RH. It is also important to measure the weight of the setup at the same conditions as the weight of the blank so that they are comparable.

Once the blank mass is known, the gas feed of known humidity is connected to one opening of the flask cap, coming out of the other while being in contact with the sorbent. The humidity of the humidifier outlet gas is measured by a relative humidity sensor, and the bed temperature is measured by a thermocouple in contact with the bed. The bed temperature can be controlled by immersing the flask in the water bath. The humidity on the bed can be tuned by combining the humidifier outlet gas of known RH with a selected amount of pure N<sub>2</sub> flow, while taking into account the temperature inside the bed.

The weight of the capped flask containing the bed is measured repeatedly over time until no significant mass change is detected, at which point equilibrium has been reached. The adsorption capacity is then obtained based on the mass difference of the bed before and after the experiment, as shown in Equation 24. The fact that only small quantities of around 1 gram of sorbent are used magnifies the error in the mass measurement, but ensures that all of the sorbent particles in the bed are in contact with the gas. Similar to the breakthrough method, single and multiple equilibrium experiments were performed.

$$q_{eq} = \frac{m_{equilibrium} - m_{blank}}{m_{blank} - m_{setup}} \cdot \frac{1}{MW_W} \quad (24)$$

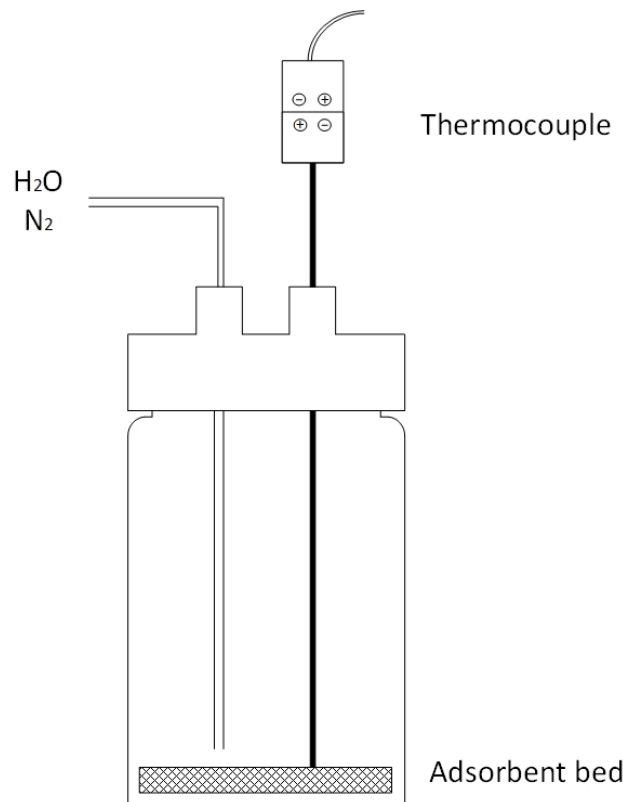


Figure 16: Diagram of the simplified setup.

## 4 Results and discussion

### 4.1 Experimental methods validation

Over sixty breakthrough experiments were performed at different values of temperature and relative humidity as described in subsection 3.2. Initially only these two parameters were varied but later it turned out to be necessary to study different values of flowrate. The main difference with existing literature data (see subsection 2.1) is that in these experiments the temperature was kept constant for each set of RH values, which shows the isothermal behavior of the system.

According to basic adsorption theory, the only process variables that can affect the equilibrium adsorption capacity of a given adsorbate are effective adsorbate concentration, sorbent temperature and the presence of a different adsorbate in case of competitive adsorption. Thus initially, the experiments were being performed without taking into consideration the flowrate as a variable that could affect the equilibrium results. However, due to inconsistent results it was decided to study its effect on the calculated capacity value. Figure 17 shows the calculated values of equilibrium capacity at 15°C for two different values of flowrate. Please note: the effects of the change in flowrate on pressure and temperature were accounted for in the calculation of the mole fraction, so the difference in capacity is not due to these.

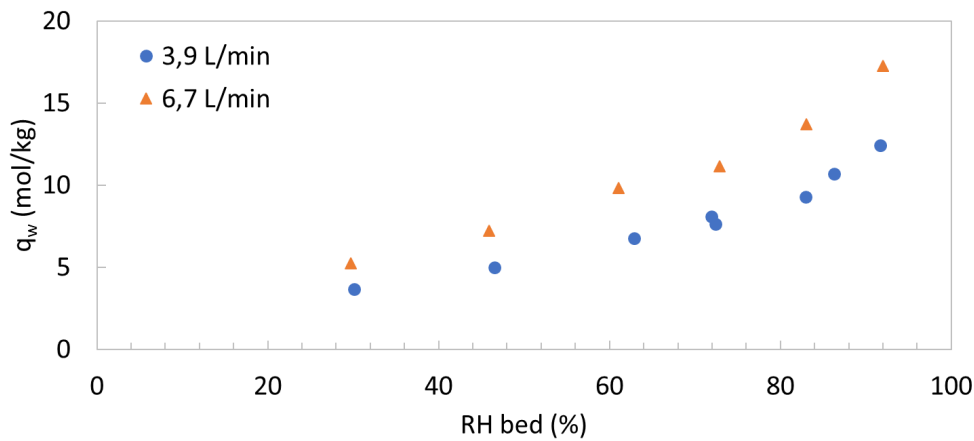


*Figure 17: Water adsorption equilibrium data at 15°C for two different values of flowrate.*

The results clearly show that the apparent value of the adsorption capacity increases significantly with the flowrate used in a consistent manner. To better understand this, another set of experiments was performed by measuring the equilibrium capacity at the same value of RH for different values of flowrate. The results are shown in Figure 18.

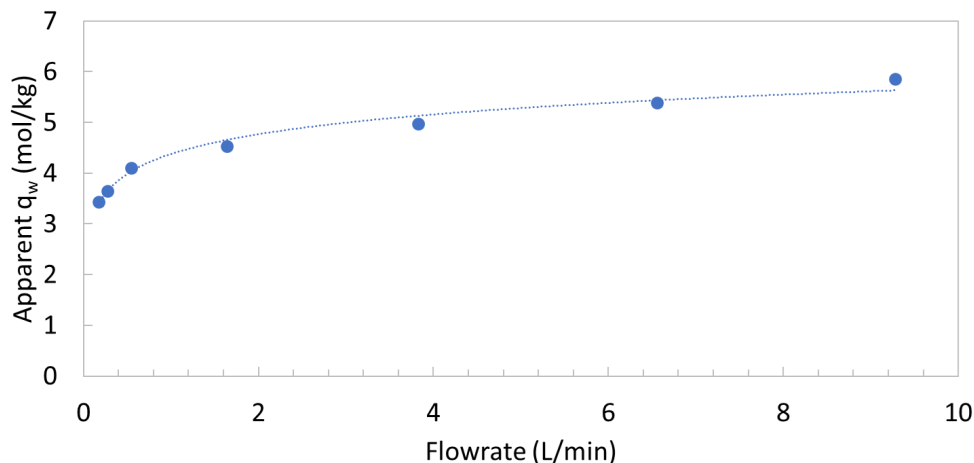


*Figure 18: Water adsorption equilibrium data at 20°C for varying values of flowrate.*

Six equilibrium experiments were performed for values of flowrate ranging from the highest to the lowest values possible in the setup. None of them got the same result, in fact they seem to show a quasi-logarithmic behavior of the apparent capacity with the flowrate. This unexpected result point to something being wrong with the experimental method or the processing of data. Changing the flow after equilibrium had been reached showed no effect on the calculated capacity. This made it clear that the apparent dependency of the equilibrium capacity with the flowrate is not real, it is instead an artifact of the method.

One hypothesis put forward was that the response time of the sensors, which was know to take up to one minute, was affecting the measurement differently depending on the flowrate. The response of the sensor to changes was characterized and fitted to a first order response time model. A deconvolution analysis was performed to remove the effect of response time mathematically from the RH signal, after which the capacity was recalculated. The details can be found in subsection A.3. In summary, the effect of the response time on the RH measurement did have an effect but was not significant enough to account for the flowrate dependency. It did, however, considerably reduce the error when studying the response of the sensors when in the empty vessel.

The most important experimental test performed regarding this issue was the use of a sorbent that could be measured using a breakthrough method and a gravimetric method at the same time. To do this the fresh sorbent was weighed, then put into the big setup where the breakthrough experiment was performed. Then, the sorbent particles were recovered and weighed again to obtain the capacity from the difference in mass. Due to the small size of the Lewatit sorbent particles and its tendency to stick to any surface, it's nearly impossible to recover all the particles when weighing and putting them inside the setup back and forth. Zeolite UOP 3A was used instead, because its big particle size makes it easy to move around and ensure that no particles are lost during displacement. The difference between the two sorbents can be observed in Figure 19. Note how in the case of the zeolite it is easy to keep track of how many particles are being used during the experiment, ensuring no loss of material occurs, whereas in the case of Lewatit it is almost guaranteed to occur.



(a) Lewatit VP OC 1065<sup>TM</sup> spheres in two different containers.

(b) Zeolite UOP 3A spheres.

**Figure 19:** Lewatit and zeolite sorbent particles in the quantity of approximately 1 gram.

The procedure was performed at two different values of flowrate, one being 17 times the value of the other. The results are shown in Table 2. The gravimetric measurements are sufficiently precise since they are in agreement with each other for the two different flowrates. However, the breakthrough measurements show a difference of more than twice the value with respect to each other and are also far from the gravimetric measurement. This represents how lacking the breakthrough method is in terms of precision. In addition, if we assume that the gravimetric measurements are accurate, it also shows a notable lack of accuracy.

**Table 2:** Comparison of water capacity measurements of zeolite UOP 3A for two different values of flowrate using two different measurement methods.

| $\phi_V$ (L/min) | Adsorption capacity of water (mol/kg) |                          |
|------------------|---------------------------------------|--------------------------|
|                  | Gravimetric measurement               | Breakthrough measurement |
| 0.55             | 6.3                                   | 8.6                      |
| 9.28             | 6.6                                   | 3.4                      |

A small change in temperature can greatly affect the RH of a gas. To check if the issue with the breakthrough results

stems from a problem with the temperature measurement, the results of these tests were re-evaluated by using temperature values from different sensors for the same experiment. However, the temperature measurements of the RH sensor and the thermocouple returned a similar result. To check if a temperature correction would fix the issue, the values of capacity were also recalculated by introducing negative and positive offsets on the temperature measurements of the inlet and outlet of up to 5°C, but the value was never the same for the two different flowrates. Correcting for the response time of the sensors barely had any effect on the result.

Regardless of their validity, four different sets of isothermal breakthrough experiments were performed at different bed temperatures: 15°C, 20°C, 25°C and 45°C. All of these were obtained from the same batch of Lewatit, on the same setup and at the same gas flowrate (3.9 L/min). The four experiment sets are shown in Figure 20 together with the previous results from Veneman et al.

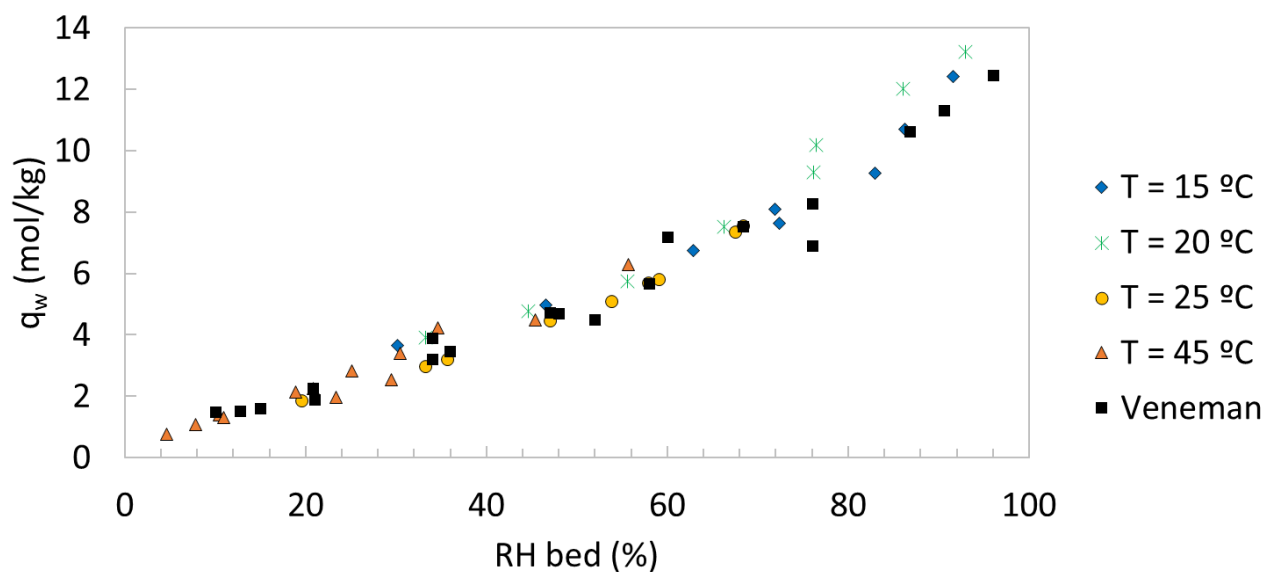


**Figure 20:** Results of water adsorption equilibrium data at different temperatures and constant flowrate using the breakthrough method, together with Veneman's literature data. Note: Veneman's data is not isothermal[1].

No trends appear to be present with temperature. This is unexpected, because in one of the tests the temperature of the bed was reduced suddenly after equilibrium had been reached and the breakthrough curve showed adsorption taking place after that (mole fraction of water in the outlet was decreased for a short time). That behavior points to a higher adsorption capacity at lower temperatures which is not apparent in these results.

Veneman et al. used the data from Natalia Frigka [42], but she used a different data processing method than the one presented in this work (see subsection 3.2). However, she still found similar results to the ones from this study.

Regarding the measurement of CO<sub>2</sub> adsorption capacities, Natalia found that the CO<sub>2</sub> capacity obtained from breakthrough measurements from the same setup was replicable using a TGA method [42]. Since CO<sub>2</sub> capacity measurements are obtained using a different measurement method, this means the problem is not the setup itself but rather the measurement method used in combination with it.

In summary, the results of the breakthrough method are inaccurate, imprecise and inconsistent with the flowrate used. It also has replicability issues due to the effect of sensor positioning on the temperature and RH measurements. For these reasons, the method is unsuitable for measuring water adsorption equilibrium capacities. Figure 20 shows the similarity of this study's water capacity data obtained from breakthrough experiments to Veneman's data, obtained using the same setup and method. This makes it clear that previous literature data bears the same problems.

The exact reason why the breakthrough method performance is so poor is yet unknown. In order to find out, one could do several more checks in the setup. For example, check if using an RH sensor with a different measurement principle such as a resistive or thermal sensor instead of a capacitive one yields better results; or bypass a very small part of the reactor gas feed and measure the RH in that point to see if the result changes.

In any case, it was decided not to pursue this method further and instead develop a gravimetric method that

could be used with Lewatit, as described in subsection 3.3. In order to check the validity of that method, a similar test as that of the zeolite was performed for Lewatit in the small setup, using the same conditions and flowrates as in Table 2. The equilibrium capacity measured this way was nearly identical for both values of flowrate. The result is shown in Figure 21 under the name "Flow check".

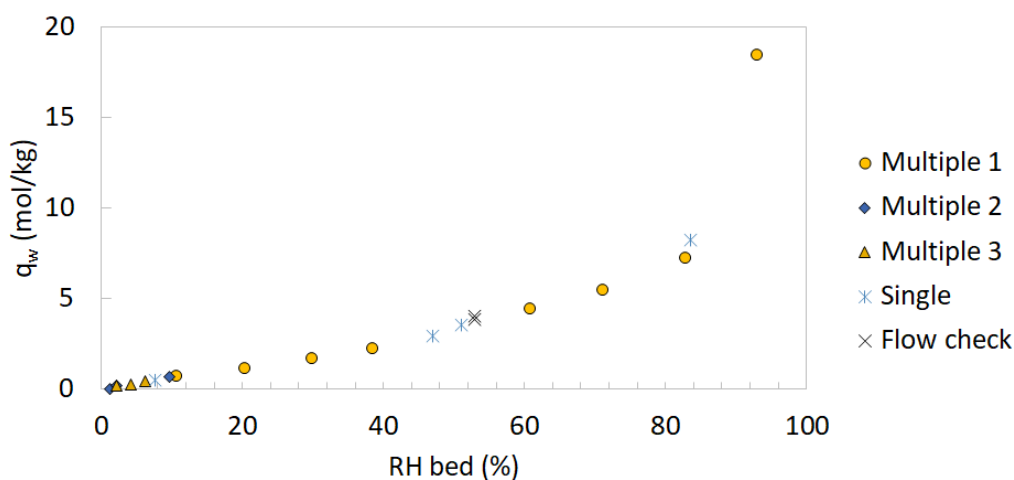


**Figure 21:** Results of water adsorption equilibrium data at ambient temperature, showing which data points were obtained separately and which were obtained in a multiple equilibrium experiment via the gravimetric method.

The precision of the method can be appreciated in this graph, since the values of capacity obtained at similar RH are quite close to each other. In addition, the capacity results of multiple equilibrium experiments are in good agreement with those of single equilibrium experiments. Due to its superior precision and consistency, the results of the gravimetric method are treated as valid during the following parts of this work, unlike those of the breakthrough method. In addition, the gravimetric method can be easily used to measure the capacity in the low RH range since it does not require measuring the humidity of the outlet gas.

## 4.2 Gravimetric data discussion

Three data sets of equilibrium adsorption capacities of water were obtained using the gravimetric method, each at a different temperature. The results are shown in Figure 22.

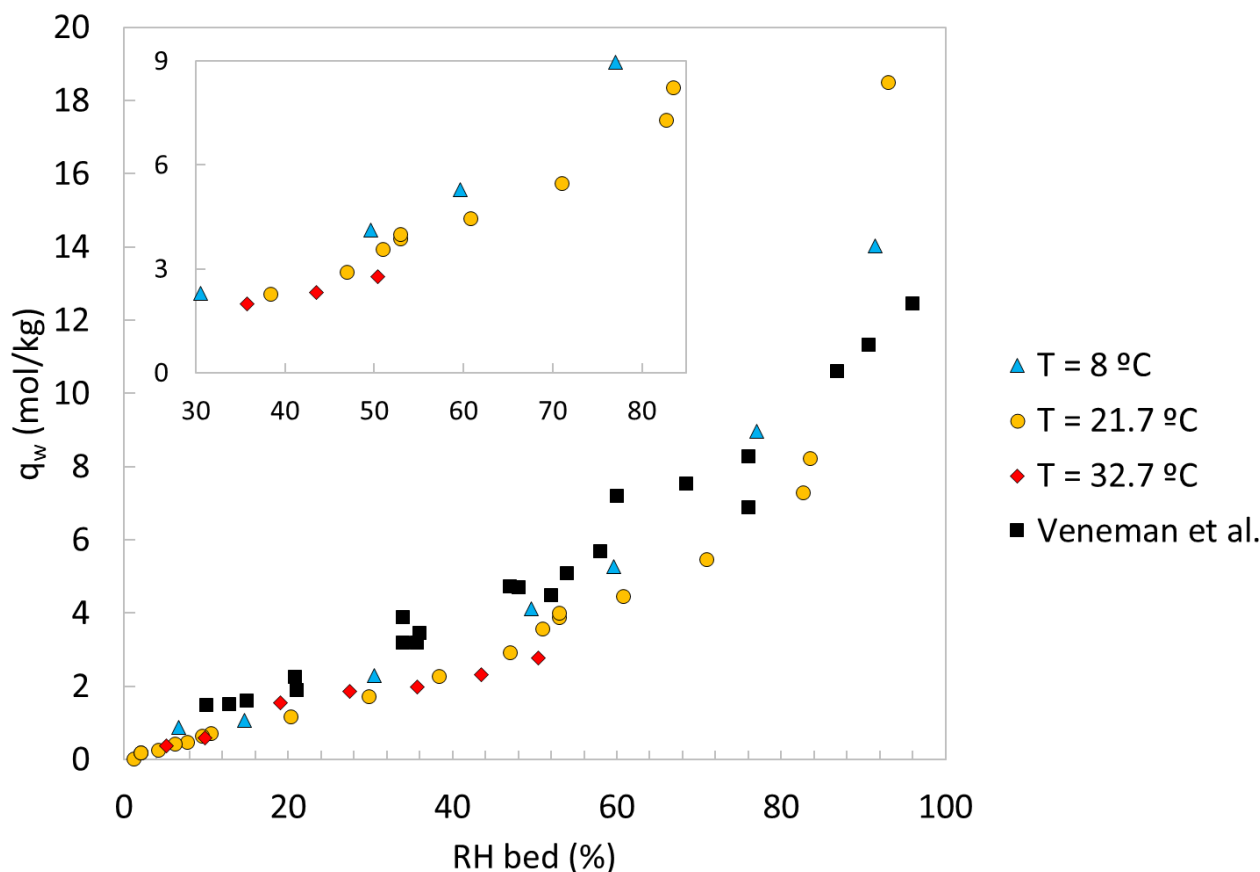


**Figure 22:** Results of water adsorption equilibrium data at different temperatures using the gravimetric method, together with Veneman's literature data. The small graph is a zoom in the region of  $RH = 30\text{--}85\%$ . Note: Veneman's data is not isothermal[1].

From the capacity values in the low RH region we observe an apparent lack of a monolayer knee curve, which implies an extremely weak adsorbent-adsorbate interaction in terms of energy. This shows that the Lewatit-water system presents a Type V adsorption isotherm according to the Aranovich-Donohue classification, as depicted in Figure 5b. This means that the BET model cannot represent the data adequately [28]. The presence of a third sorption stage in which the adsorption capacity diverges upwards becomes apparent around  $RH = 80\%$ .

The gravimetric method data show the temperature trend expected from the exothermic nature of the adsorption process. The equilibrium capacity decreases with increasing temperature, because the higher temperature increases the excitation of the molecules, increasing the distances and reducing the attractive forces between them. This is in stark contrast with data from the breakthrough method in this work and that of Veneman et al. [1], in which there are no clear trends in temperature. This probably stems from the poor precision of the method they used. Those data overestimate the capacity in most of the RH range but underestimate it throughout the 3rd sorption stage.

It is important to note that out of the three temperature data sets studied, the one at ambient temperature ( $T = 21.7^\circ\text{C}$ ) is to be trusted the most. The reason is that it did not require the use of a water bath to keep it under the right temperature, and the temperature over the bed was homogeneous, unlike the other two. The blank weight is easy to measure because it needs not include the possible effects of water adsorption over the glass flask or the flask temperature affecting the weight measurement. The dataset at  $T = 32.7^\circ\text{C}$  is to be trusted the least because the temperature of the flask was affecting the weight measurements patently during the experiment. For this reason, the dataset at  $T = 32.7^\circ\text{C}$  will not be used in the development of isotherm models in further sections.

The maximum value of capacity measured ( $q_w = 18.5\text{ mol/kg}$ ,  $RH = 93\%$ ,  $T = 21.7^\circ\text{C}$ ) warrants some discussion. The value is higher than the previous maximum value from literature ( $q_w = 12.5\text{ mol/kg}$ ) [1]. Based on the value of pore volume of the material (see Table 1), the maximum possible adsorption capacity is  $20.5\text{ mol/kg}$ . That means the maximum value obtained in this work is still below the one that would be obtained in case that all the pores were filled with condensed water.

One could think that the presence of a significant amount of water could be causing the increase in CO<sub>2</sub> capacity via absorption of CO<sub>2</sub> in the water condensed in the pores. However, assuming that the absorption capacity of the condensed water is equal to that of free water at the same temperature, the amount of CO<sub>2</sub> absorbed would not surpass 0.01 mol of CO<sub>2</sub> per kilogram of sorbent. Experiments showed that the increase can be upwards of 0.5 mol/kg [1], so the enhancement mechanism cannot be explained this way.

Even though these results seem to be enough to characterize the system well, there is a lot of room for improvement in future research on this topic. Ideally, the sorbent would be in a flask of a material that does not change its weight with temperature or in contact with water, which would directly eliminate the main source of uncertainty. Performing any future experiments by measuring the humidity of the gas in the humidifier outlet instead of in the gas feed is recommended to measure the low RH range correctly and reduce systematic uncertainty.

The precision and consistency of the method have been proven in this work, but the accuracy has not. To do this one could perform multiple equilibrium experiments with a material of well-known capacity and compare the results to literature. In addition, even though the precision of the method seems good, it would be better to perform a standard deviation analysis of the measurements by performing multiple measurements for the same combination of RH and temperature.

As of how the setup is now, high RH measurements are not possible at ambient temperature or higher. High RH values require humidifying the feed gas at elevated temperature to reach the required value of water pressure and a way to avoid condensation in the tubes leading to the flask by keeping them warm enough. One possible solution could be to use metal tubing with heat tracing connected all the way to the bed.

One alternative to all of these possibilities would be the use of an enhanced gravimetric method that circumvents the problems of the current one, such as the one described in the work of Portugal et al.[27]. By using different salt saturated aqueous solutions and placing the adsorbent bed in a bag inside a closed flask containing the solution in combination with a temperature bath, one can perform these experiments at controlled humidity and temperature without having to account for uncertainty of the RH measurement or blank weights.

## 4.3 Isotherm model

### 4.3.1 Experimental fit results and isotherm model selection

The isotherm models described in subsection 2.2.2 were fitted to the gravimetric method data at ambient temperature. The BET and GAB models are derived theoretically and their parameters have clear and well-founded physical meaning, which allows us to interpret the properties of the system if the model is a good fit for the data. The Aranovich model and its modifications are of a more empirical nature and thus have less theoretical explanatory power, but are more versatile in the types of data they can fit and work in a wider range of activity.

The fitting procedure applied to the data was based in the work of Timmerman [28]. Since the interaction between Lewatit and water is very weak, the fit parameters cannot be derived from graphical analysis and thus a nonlinear fitting algorithm was used. The theoretical model fits are shown in Figure 23 and the parameters are shown in Table 3. The semiempirical model fits are shown in Figure 24 and the parameters are shown in Table 4.

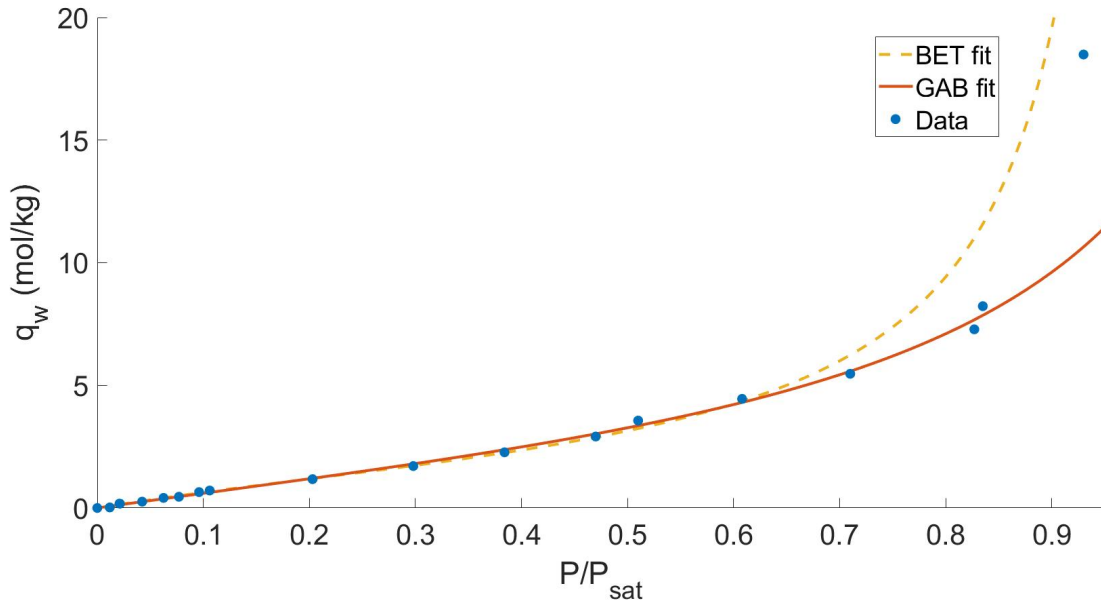


**Figure 23:** Theoretical adsorption isotherm model fits of the gravimetric method results at  $T = 21.7^{\circ}\text{C}$ .

**Table 3:** Fitting parameters of the theoretical models.

| Parameters                  | BET   | GAB   |
|-----------------------------|-------|-------|
| Range of fit (%RH)          | 5-40% | 5-85% |
| $C$ (-)                     | 3.55  | 2.37  |
| $q_m$ (mol/kg)              | 2.02  | 3.26  |
| $k$ (-)                     | -     | 0.79  |
| $R^2$ (within range of fit) | 0.998 | 0.995 |

As expected, the BET model describes the data well within its applicability range, but is not adequate to represent the relevant range of RH. The GAB model, however, shows a good fit to the data with a high coefficient of determination ( $R^2 > 0.99$ ). None of the two satisfactorily covers the whole range of humidity but GAB covers most of it.

Parameter  $C$  characterizes how pronounced the form of the monolayer knee curve is at the beginning of the RH range, which corresponds to how strong the first adsorption stage is. The values of  $C$  are very low (close to unity) which implies that the adsorption is quite weak. The energy state of molecules adsorbed on the monolayer is similar to that of molecules in the multiple layers above it. In terms of enthalpy this means  $H_1 \approx H_m$ .

Parameter  $k$  characterizes the upswing of the curve starting in the second sorption stage. Its value is quite lower than unity, which means that the energy of the particles adsorbed in the multilayer is notably higher than on the comparable liquid state. In combination with the low value of  $C$ , we can infer that this applies to the molecules adsorbed in the monolayer as well. In terms of enthalpy this means  $H_1 \approx H_m \neq H_L$ .

In terms of physical meaning, parameter  $q_m$  is more reliable than the others [28]. The value of  $q_m$  obtained from the GAB fit is remarkably close to that obtained previously for CO<sub>2</sub> adsorption over Lewatit ( $q_m, \text{CO}_2 = 3.4$ ) [23].

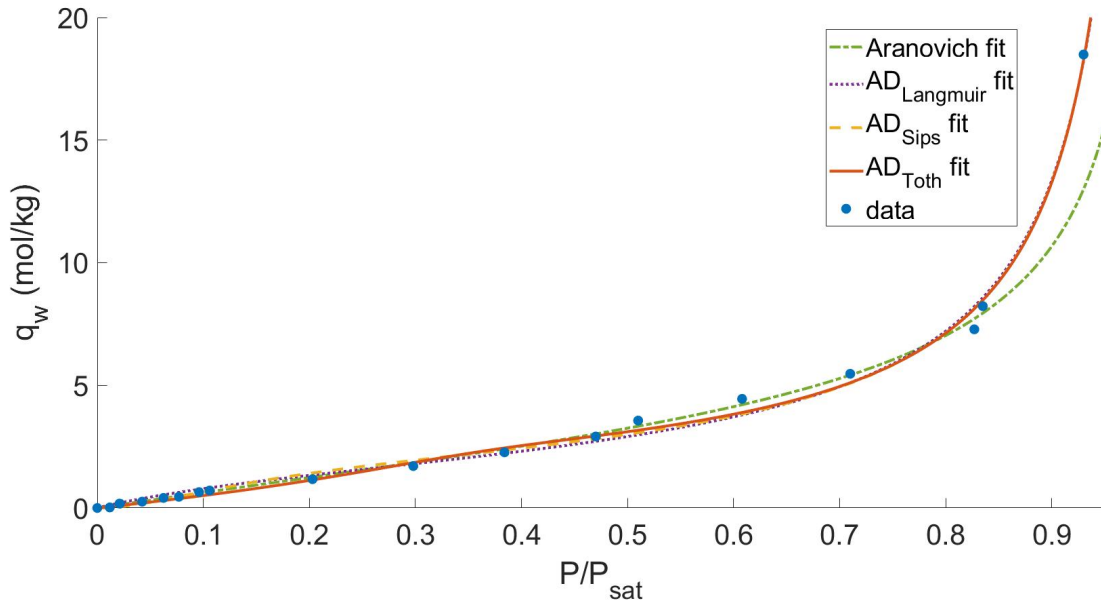


Figure 24: Semiempirical adsorption isotherm model fits of the gravimetric method results at  $T = 21.7^{\circ}\text{C}$ .

Table 4: Fitting parameters of the theoretical models.

| Parameters                  | Aranovich | AD(Langmuir) | AD(Sips) | AD(Toith) |
|-----------------------------|-----------|--------------|----------|-----------|
| Range of fit (%RH)          | 5-95%     | 5-95%        | 5-95%    | 5-95%     |
| $b$ (1/Pa)                  | 468       | 4.42E-05     | 6.93E-05 | 2.73E-05  |
| $q_m$ (mol/kg)              | 0.010     | 2.34         | 1.79     | 1.68      |
| $d$ (-)                     | -         | 0.85         | 0.89     | 0.90      |
| $n$ (-)                     | -         | -            | 0.54     | -         |
| $t_h$ (-)                   | -         | -            | -        | 8.41      |
| $R^2$ (within range of fit) | 0.969     | 0.994        | 0.995    | 0.996     |

It is clear that the Aranovich model is not a good fit for the whole RH range, even though it performs just as well as the GAB model on the same range (5-85%). The modifications of it, however, perform reasonably well for the entire RH range. All three of them have a similarly good fit but AD(Toith) performs the best.

The values of parameter  $b$  represent the adsorption energy of the system. They are all very low, which again represents the weak interaction between Lewatit and water.  $q_m$  values are lower than for GAB, but they cannot be trusted as much as that one due to the strong empirical component of these models.

The value of parameter  $d$  is directly proportional to the divergence in the value of capacity as RH increases. The value is higher than in the basic Aranovich model (in which  $d = 0.5$ ), but lower than the maximum value possible (equivalent to the one predicted by BET). The  $n$  parameter of the Sips isotherm is considerably lower than 1, which implies a very heterogeneous surface. The  $t_h$  parameter of the Toth isotherm is in agreement since it is quite higher than 1.

In order to characterize the temperature dependent adsorption behavior of the Lewatit-water system, an adequate isotherm model must be selected as the basis. Ideally the model will have a high goodness of the fit (Represented by the  $R^2$  parameter) and a strong physical meaning. The GAB model fits these requirements best out of the models described in subsection 4.3.1, due to its theoretical explanatory power in combination with its high goodness of the fit for most of the RH range. In addition, the residual plot of the GAB model shows a random distribution, which implies that the model explains the different trends in the data adequately (see Figure 25).

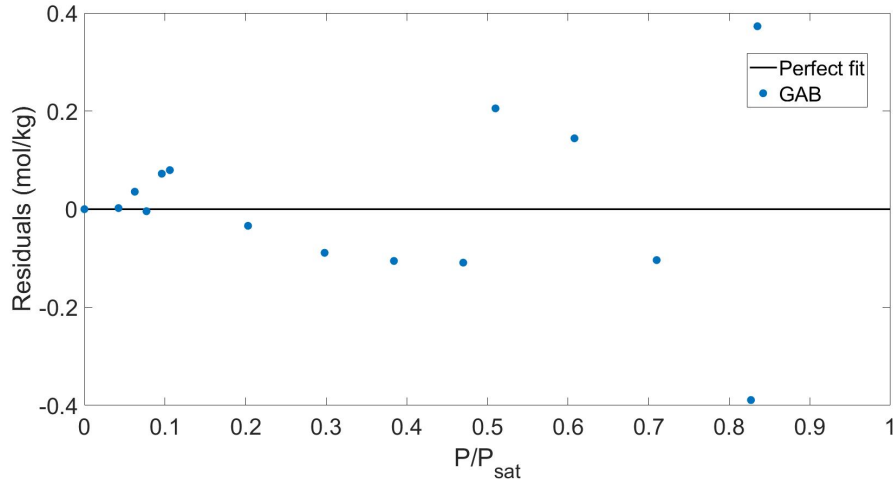


Figure 25: Residual plot of the GAB model fit of the data.

### 4.3.2 Temperature dependent model

A temperature dependent isotherm model was developed using the GAB model. The basis of the model are the two equilibrium capacity data sets obtained at temperatures of 8°C and 21.7°C. The data set at 32.7°C was not included due to its short range of RH. This means that the thermodynamic parameters of the temperature dependent fit were obtained from a two-point regression (see subsection A.6), which strongly limits the validity of the model. One must be extremely careful when extrapolating this model outside of the temperature range of the data used ( $T = 8 - 21.7^\circ\text{C}$ ). Ideally more data at different temperatures ought to be incorporated in the model for future research.

Since only two temperature data sets are used, the dependency of  $q_m$  with temperature cannot be proved or disproved. It was thus assumed to be constant with temperature, and obtained as a parameter from the value which maximized the goodness of the fit for both temperatures combined. The results of the fit are shown in Figure 26, and the model parameters can be found in Table 5. In order to assess the goodness of the fit the Normalized Standard Deviation (NSD) of the model from the data was calculated according to Equation 25, and the parity plot is shown in Figure 27. As can be observed, the data shows no significant deviation from the model.

$$NSD = \sqrt{\frac{\sum [(q_{exp} - q_{model}) / q_{exp}]^2}{N - 1}} \quad (25)$$

Where  $q_{exp}$  is the experimentally measured equilibrium capacity,  $q_{model}$  is the equilibrium capacity predicted by the model and  $N$  is the total amount of data points in the model.

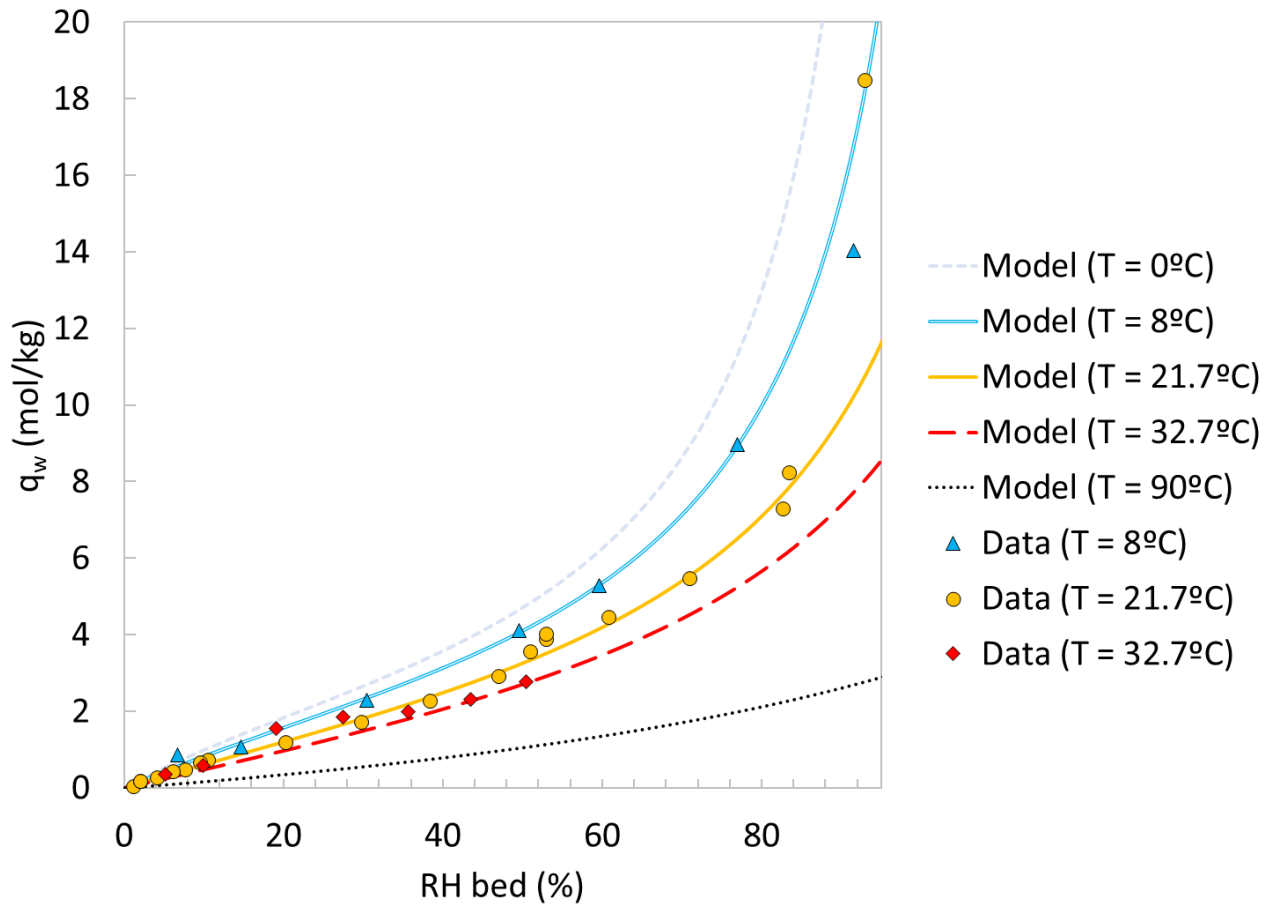


Figure 26: Temperature dependent isotherm model and experimental data.

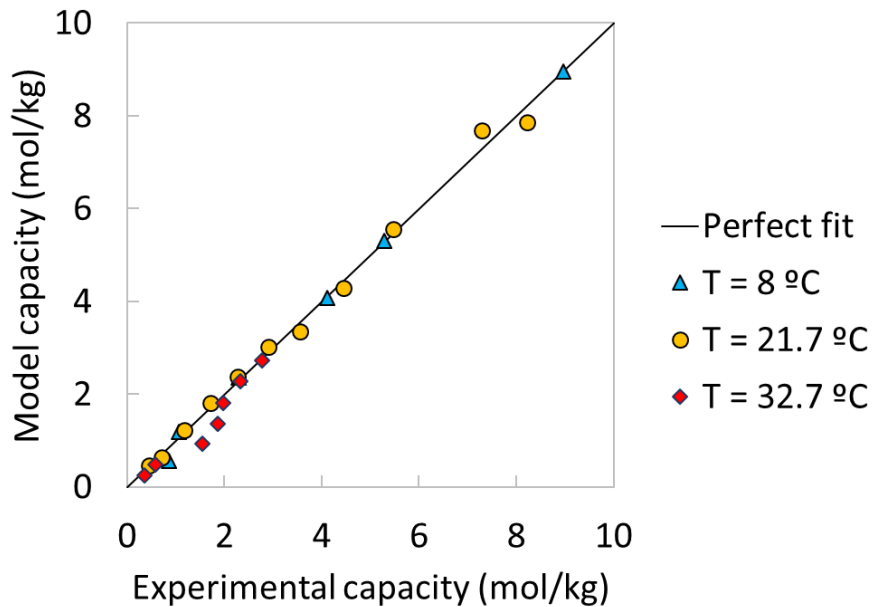


Figure 27: Parity plot of the temperature dependent model within the RH range of validity.

Table 5: Fitting parameters of the temperature dependent isotherm model.

| $\Delta H_C$ (kJ/mol) | $\Delta H_K$ (kJ/mol) | $C_0$ (-) | $k_0$ (-) | $q_m$ (mol/kg) | NSD   |
|-----------------------|-----------------------|-----------|-----------|----------------|-------|
| 12.2                  | 5.9                   | 1.72E-02  | 7.14E-02  | 3.10           | 15.8% |

The value of  $\Delta H_C$  is positive as expected, meaning the molecules are bound more strongly than those in the multilayer. However it is low compared to other values from literature[28], which indicates the average energy state of molecules in the monolayer is not much higher than in the multilayer.

On the other hand, the positive value of  $\Delta H_k$  is unexpected, since it would mean the molecules in the multilayer are bound less strongly than those in the liquid[29], which should not be the case as shown in Figure 6. Indeed, the fact that  $k < 1$  already implies the opposite[28]. It is most likely that this behavior stems from having obtained the value from a two-point linear regression. Probably adding more isothermal data will show that the value of  $k$  actually increases with temperature instead of decreasing, thus changing the sign of  $\Delta H_k$ .

This is further proof of the limited explanatory power of the temperature dependent model, and that more data points at different temperatures are required to come to a definite conclusion. However, if this behavior persists when incorporating more data in the model, it would point to the presence of an unknown endothermic phenomenon taking place simultaneously with the adsorption; i.e. an absorption or dissolution process, or an interaction of the water with the amine sites.

Theoretically the value of the isosteric heat of adsorption ( $\Delta H_{is}$ ) could be obtained via Equation 7 [29]. However, for the reasons stated above it is not recommended to do so. Instead, the value has been calculated from the difference between the adsorption heat and the vaporization heat of water.

The adsorption heat of water over Lewatit ( $\Delta H_{ads,w}$ ) has been obtained by applying the Clausius-Clapeyron relation as described in Equation 8 in combination with the temperature dependent GAB isotherm at two different temperatures ( $T = 8^\circ\text{C}$ ,  $T = 21.7^\circ\text{C}$ ). The results are shown in Figure 28.

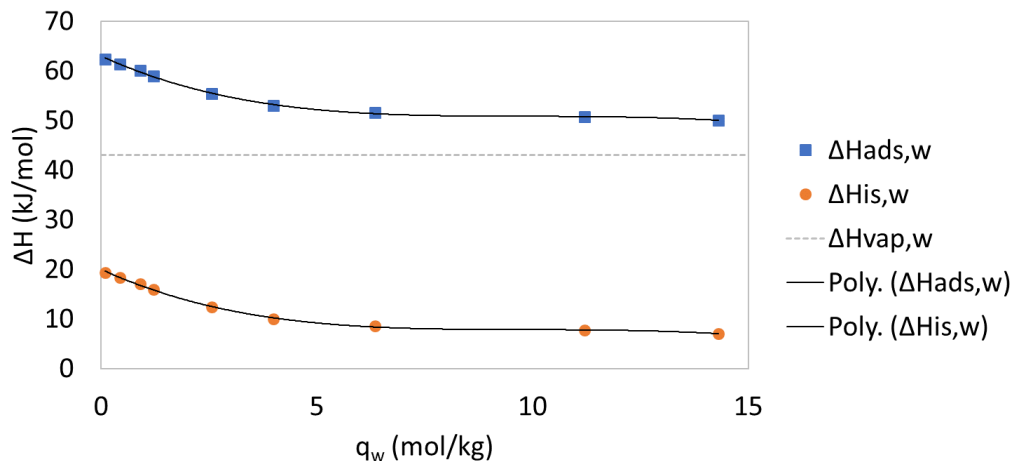


**Figure 28:** Heat of adsorption of water over Lewatit, enthalpy of vaporization and isosteric heat for different values of adsorption capacity.

The value of  $\Delta H_{is}$  is within the expected range, and its average is nearly identical to the value of parameter  $\Delta H_C$ . Literature values are similar for isosteric heat of water adsorption on other materials such as montmorillonites [43], zeolites [32] and rice [44]. The results are nearly identical to those that would be obtained by using the experimental data directly instead of the model.

The reason why  $\Delta H_{ads,w}$  decreases with the value of capacity is due to the difference in the enthalpy of molecules in the monolayer and multilayer and the different degree of monolayer coverage. At increasing RH the most active sites become filled and sorption occurs on progressively less active sites, giving lower heats of sorption [29]. The degree of occupation of the monolayer for different temperatures was calculated according to Equation 9 is shown in Figure 29 to characterize the jamming phenomenon predicted by the GAB model.

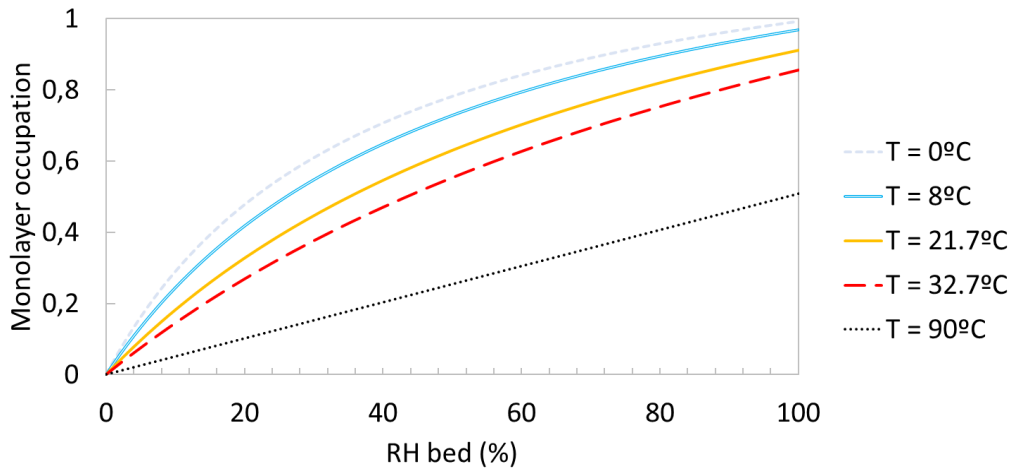
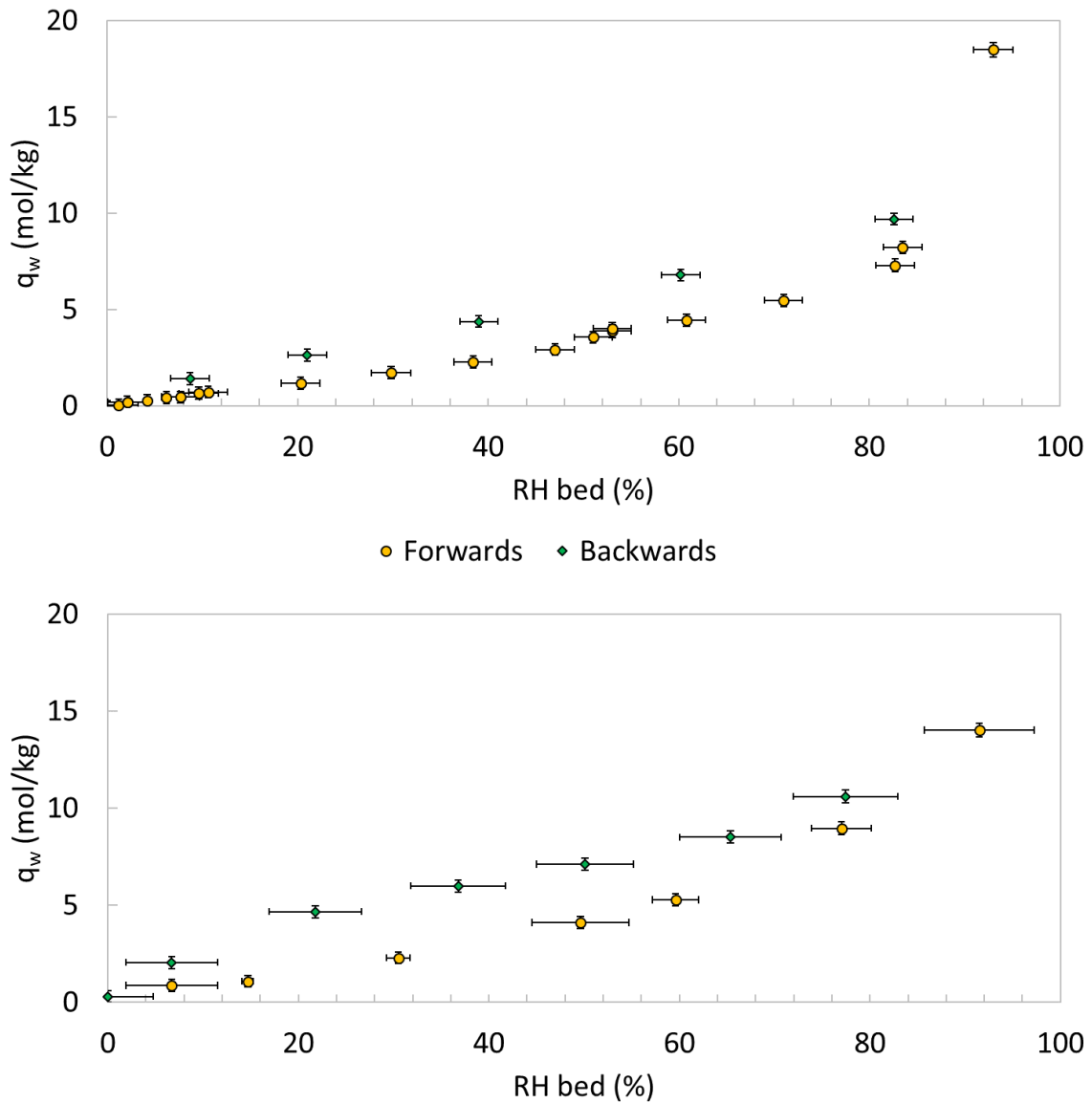


Figure 29: Degree of monolayer occupation predicted by the model at different temperatures.

#### 4.4 Adsorption hysteresis

The results in this section were obtained by applying the method described in subsection 3.3 to perform multiple equilibrium experiments. First the highest RH value that can be obtained with the current setup was reached (RH  $\approx$  93%). The hysteresis loop is then started by lowering the humidity of the gas feed. When equilibrium is reached, the capacity is measured and the RH is lowered again, obtaining multiple values of equilibrium capacity. This way the hysteresis loop of the system was characterized for the temperatures of T = 9°C and T = 21.7°C as shown in Figure 30. A crucial consideration is that eventually the value of RH = 0% (pure nitrogen) was reached and the values of capacity obtained were effectively zero, which demonstrates the reversibility of the hysteresis in the system.



**Figure 30:** Hysteresis behavior of the system shown by the adsorption equilibrium capacity of water when going forwards and backwards in RH for  $T = 21.7^\circ\text{C}$  (top) and  $T = 8^\circ\text{C}$  (bottom).

The hysteresis loop seems closest to a type  $H_3$  loop as depicted in Figure 8. Strikingly, hysteresis was maintained for an extremely wide range of humidity, at least for the entire range tested ( $\text{RH} = 7\text{-}93\%$ ). This would seem to suggest that pore condensation is a major component of the adsorption mechanism of the system, particularly since the capacity can be sometimes twice as much going backwards in the loop than it is when going forwards.

This is in stark contrast with the conclusions of Veneman et al.[1], who deduced that pore condensation was not expected to be the main mechanism during the range of  $\text{RH} = 10\text{-}60\%$  from the analysis of the pore distribution of Lewatit. To understand this, the pore size of the material will be discussed in relation to the results. Figure 31 shows the value of the Kelvin radius calculated via Equation 15 for adsorption and desorption, in context with the experimentally observed hysteresis bounds.

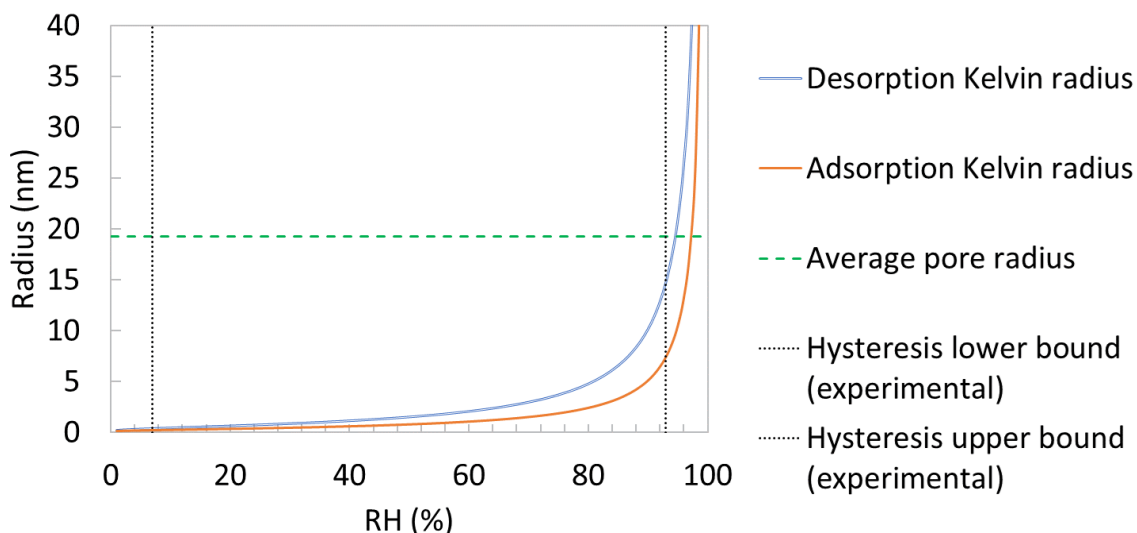


*Figure 31: Kelvin radius of the Lewatit-water system.*

Based on the RH values at which the Kelvin radii for adsorption and desorption conditions meet the average pore radius, pore condensation should only become significant in the range of RH = 94-98%. This seems to imply an extremely wide pore size distribution, with sizes ranging from over twenty nanometers to nearly zero. One possibility to describe this behavior could be a bimodal pore volume distribution with a large concentration of micropores as well as mesopores. However, the absence of a knee at the beginning of the adsorption curve suggests a very small micropore volume. This is in accordance with Veneman et al. who estimated the micropore volume of Lewatit to be insignificant[1].

One possible answer to this substantial discrepancy between theory and results is that the hysteresis in the system is not being caused entirely by pore condensation but by something else instead. It is also possible that the Kelvin equation does not directly apply to the system due to irregular geometry of the pore system. In order to better understand the hysteresis behavior of the system, one could characterize the pore size distribution using more sophisticated methods such as mercury intrusion porosimetry. Based on those results, one could ascertain the effect of pore condensation in the system.

#### 4.5 Process design considerations

The results obtained in previous sections have important implications for the conceptual design of a DAC adsorption-desorption cycle. In this section the effects of hysteresis on the operation of the adsorption step are discussed, as well as the trade-off situation between the energy penalty of water adsorption and the enhancement of CO<sub>2</sub> equilibrium capacity in the presence of water.

The adsorption step is expected to take around 1.5-2 hours [45], which is long enough for hysteresis to be relevant during operation. Since the gas feed of the process is ambient air, weather changes can change the RH of the feed significantly in this timescale. An increase in the equilibrium capacity caused by this can be easily predicted using the temperature dependent model developed in subsection 4.3.2, but a decrease in RH is different.

In subsection 4.4 one particular hysteresis loop of the system was studied, specifically the one starting at RH = 93%. However, the values of equilibrium capacity inside the hysteresis loop depend on the point at which the loops starts [24]. Other possible hypothetical hysteresis loops are shown in Figure 32 together with the one that was measured in subsection 4.4. Characterizing these possible loops would require performing additional hysteresis experiments on the system.

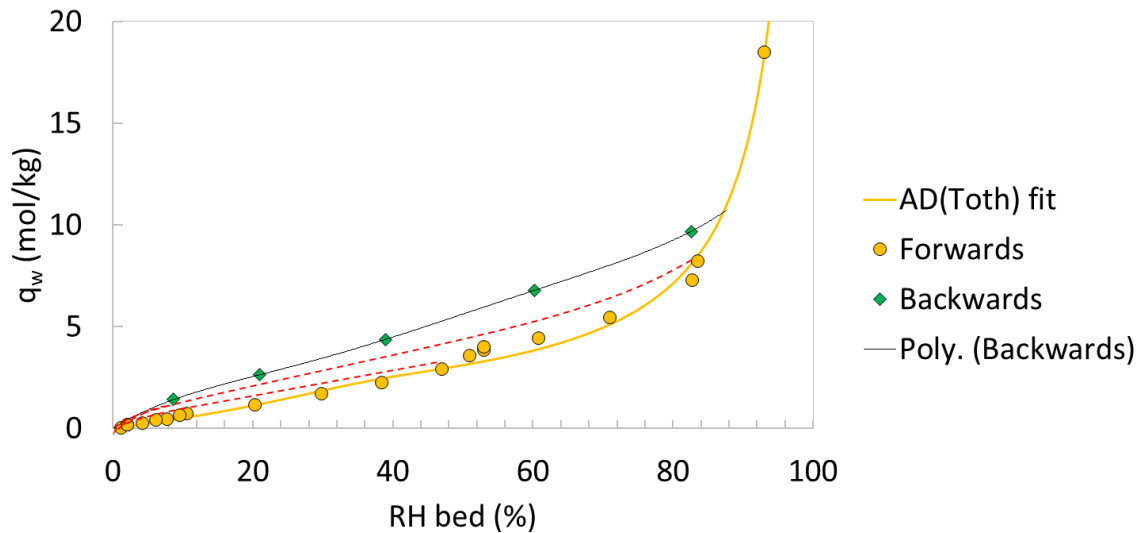


**Figure 32:** Hysteresis behavior of the system at ambient temperature. The dashed lines represent author interpretations of hypothetical hysteresis loops at different values of RH. Note: the AD(Toth) model is used to properly describe the adsorption at the higher RH range.

In case of a quick decrease in the ambient air RH caused by normal weather fluctuations, not only the equilibrium capacity of water would change but also that of CO<sub>2</sub>, since the second partially depends on the first. It is reasonable to think that a change from very high to very low RH in the feed could affect the CO<sub>2</sub> equilibrium capacity so much that the equilibrium would be suddenly reached, making it best to stop the adsorption step. Perhaps the CO<sub>2</sub> equilibrium capacity could even be exceeded, which could cause unwanted CO<sub>2</sub> desorption during the adsorption step, making it necessary to stop the adsorption step immediately. For reference, the change has been experimentally proven to be at least as big as  $\Delta_{eq}q_{CO_2} = 2.02 - 1.41 = 0.61$  mol/kg, for a change of RH = 0-75% at T = 15°C [1].

Weather RH changes are usually slower than this, but this situation could eventually happen if the plant is operated for a long enough period of time. Because of all these unknowns, it is important to obtain experimental results on the laboratory and/or pilot scale that correspond to these situations to see how the system actually reacts.

In addition, it is at this point still unknown the extent at which the CO<sub>2</sub> equilibrium capacity will be affected from a decrease in RH. It is possible that the capacity after the decrease will be different from the one expected from the adsorption experiments for the corresponding water capacity. If the enhancement mechanism was better known, it would probably also allow for making theoretical predictions of these phenomena.

Finally, the trade-off between the water penalty and the CO<sub>2</sub> capacity enhancement is to be assessed. Both equilibrium capacities of water and CO<sub>2</sub> increase with the value of relative humidity, and while the first one increases the required energy per unit of CO<sub>2</sub> captured, the second one decreases it. Thus, it is not evident which value of RH is best for minimizing energy consumption during operation. Moreover, the rate at which they increase with RH changes depends on the temperature, so this also needs to be accounted for. The adsorption capacities are represented in Figure 33 for the relevant temperature range of T = 5-40°C.

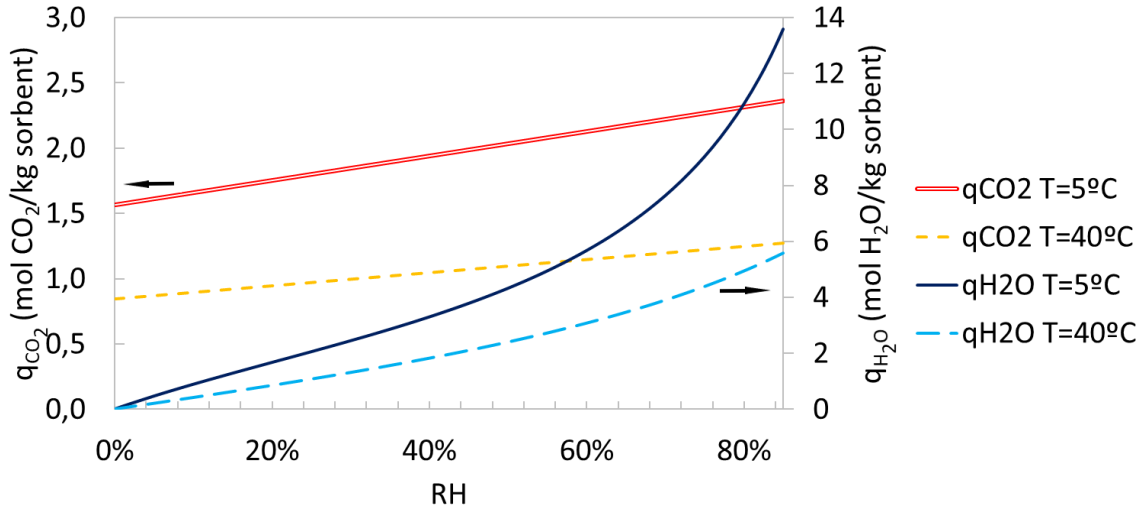


**Figure 33:** Equilibrium adsorption capacities of water and CO<sub>2</sub> versus relative humidity for the two extremes of the relevant range of temperatures.

The trade-off situation was analyzed using a simplified process model created by coupling:

- The temperature dependent model for equilibrium water capacity developed in this work, as described by Equations (4) to (6) and Table 5.
- The CO<sub>2</sub> enhancement data of Veneman et al. [1], which was fitted to a linear regression model as suggested by Wurzbacher et al.[46].
- The recommended operational parameters of Tim van Schagen[45].
- The equilibrium adsorption capacity of CO<sub>2</sub> at dry conditions and ambient concentration (400 ppm) as measured by Natalia Frigka[42].
- The heat of reaction for water desorption, calculated by using the values in Figure 6 fitted to a fourth order polynomial.
- The energy duty contributions as shown in Equations (26) to (30).

$$Q_{W,r} = \frac{\Delta q_W m_{\text{sorbent}} \Delta H_{\text{ads},W}}{\Delta q_{\text{CO}_2} m_{\text{sorbent}} MW_{\text{CO}_2}} \quad (26)$$

$$Q_{\text{sens.,sorbent}} = \frac{m_{\text{sorbent}} C_{p,\text{sorbent}} (T_r - T_{\text{init}})}{\Delta q_{\text{CO}_2} m_{\text{sorbent}} MW_{\text{CO}_2}} \quad (27)$$

$$Q_{\text{sens.,reactor}} = \frac{m_{\text{reactor}} C_{p,\text{reactor}}}{m_{\text{sorbent}} C_{p,\text{sorbent}}} Q_{\text{sens.,sorbent}} \quad (28)$$

$$Q_{\text{sens.,gas}} = \frac{\phi V_{\text{gas}} \rho_{\text{gas}} C_{p,\text{gas}} (T_r - T_{\text{init}}) t_{\text{des.step}}}{\Delta q_{\text{CO}_2} m_{\text{sorbent}} MW_{\text{CO}_2}} \quad (29)$$

$$Q_{\text{vap.,steam}} = \frac{\phi V_{\text{steam}} \rho_{\text{steam}} (\Delta H_{\text{vap},W} / MW_W) t_{\text{des.step}}}{\Delta q_{\text{CO}_2} m_{\text{sorbent}} MW_{\text{CO}_2}} \quad (30)$$

The energy duty of the process was analyzed for the cases of nitrogen regeneration for production of enriched air and steam regeneration for production of pure CO<sub>2</sub>. The main assumptions of the model are:

- The working CO<sub>2</sub> capacity is assumed to be 60% of its equilibrium value:  $\Delta q_{\text{CO}_2} \approx 0.6 \cdot q_{\text{CO}_2,eq}$
- The regeneration gas is initially at ambient temperature.
- The water capacity is at equilibrium at the end of the desorption step, since the desorption rate is much faster than it is for CO<sub>2</sub> [25].

- Since desorption is being studied at atmospheric pressure, compression energy requirements are considered negligible.
- The sensible heat of the reactor vessel is difficult to estimate since the final reactor configuration is unknown. In this model it is estimated as a function of the sensible heat of the sorbent, using the following assumption based on previous analyses[45]:  $mCp(sorbent) \approx mCp(reactor)$

The values of model parameters can be found in subsection A.4. The main result is that the lower humidity range is always the best option to minimize energy consumption of the cycle per unit of CO<sub>2</sub> captured. Thus, the trade-off is resolved in favor of minimizing the water penalty, which generally trumps the enhancement of the equilibrium CO<sub>2</sub> capacity. Sensitivity analyses showed that this conclusion holds as long as the amount of purge gas used or desorption time do not increase significantly (see subsection A.5). Additionally, this should be avoided if possible since it considerably increases total energy requirements.

In conclusion, should one have to choose a location to install a direct air capture plant with Lewatit, disregarding all other factors apart from energy requirements, the best place to do it would be the driest (in terms of the lowest RH), which corresponds to arid climates. Operating at values of humidity higher than RH = 85% becomes prohibitively expensive in terms of energy due to the sharp increase in water adsorption throughout the third sorption stage. In addition, above that value this model is no longer valid because it is outside of the range of prediction of the GAB isotherm.

The optimum operational temperature for the adsorption step was analyzed for the two different cases within the relevant temperature range of  $T = 5\text{--}40^\circ\text{C}$ . Sensitivity analyses (Figure 38) showed that for the case of nitrogen regeneration, the difference between higher and lower temperatures is not very significant as long as  $RH < 50\%$ . Sensitivity analyses showed that the optimum adsorption temperature is around  $T = 20^\circ\text{C}$ . The model results for this value of temperature are shown in Figure 34. Adsorption temperatures below  $15^\circ\text{C}$  or above  $25^\circ\text{C}$  are not recommended. Thus a dry, relatively warm location is recommended.

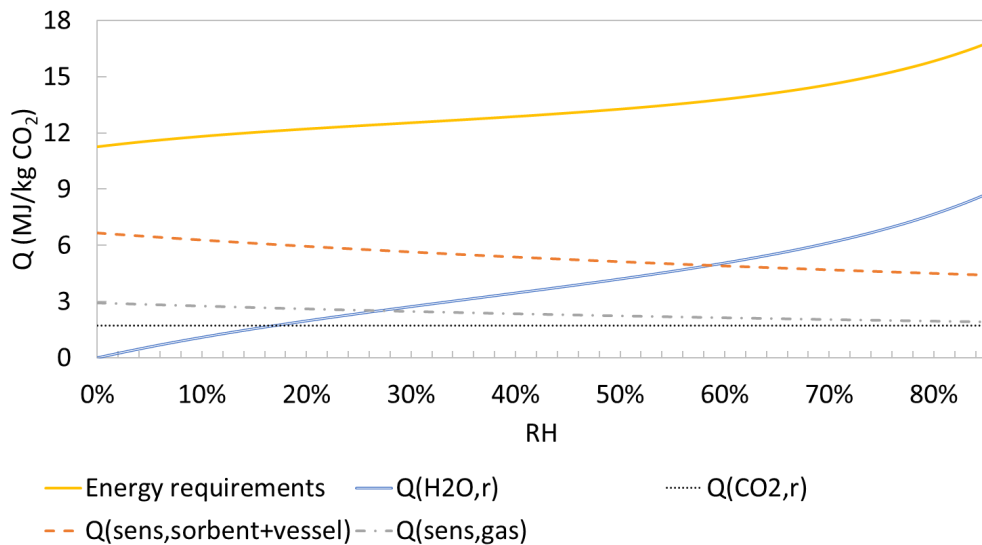


**Figure 34:** Energy requirements of the desorption step of the DAC process versus relative humidity in the bed. Results based on nitrogen regeneration for the proposed adsorption temperature of  $T = 20^\circ\text{C}$ .

For the case of steam regeneration, sensitivity analyses (Figure 39) showed that the optimum adsorption temperature depends on the value of RH. For  $RH < 70\%$  lower temperature is always better,  $T = 5^\circ\text{C}$  being the optimum. The model results for this value of temperature are shown in Figure 35. For  $RH > 70\%$ , the optimum value lies around  $T = 10\text{--}20^\circ\text{C}$  depending on RH. Temperatures higher than  $T = 20^\circ\text{C}$  are never recommended. Since lower humidity is always preferred, to produce pure CO<sub>2</sub> via steam regeneration it is best to do it in the (1) driest and (2) coldest location possible.

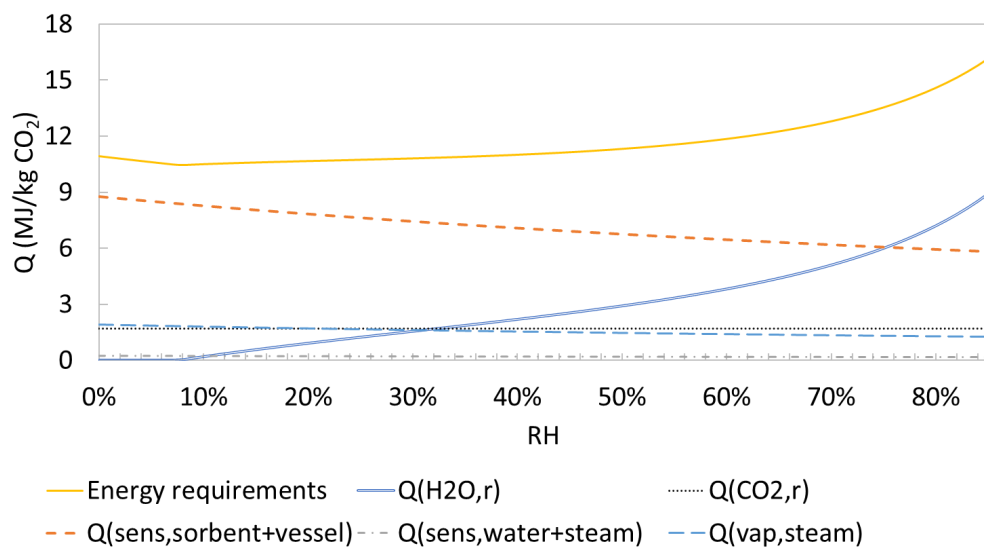


**Figure 35:** Energy requirements of the desorption step of the DAC process versus relative humidity in the bed. Results based on steam regeneration for the proposed adsorption temperature of  $T = 5^{\circ}\text{C}$ .

For a given adsorption temperature, there is an optimum value of RH at which the energy consumption is minimized. This stems from the amount of adsorbed water left on the sorbent at the end of the regeneration step. The optimum RH value increases with temperature, and for the recommended operational temperature of  $T = 5^{\circ}\text{C}$  the value is around  $\text{RH} = 8\%$ .

The conclusions of this analysis are subject to the various assumptions of the simplified model. The use of more in-depth process models which incorporate the temperature dependent isotherm model is recommended, particularly since this analysis is focused on energy and key considerations such as productivity and mass transfer rates are neglected. Regardless, the general conclusion of favoring operation at lower values of relative humidity most likely holds.

## 5 Conclusions and recommendations

### 5.1 Conclusions

The breakthrough method turned out to be too inaccurate, imprecise and inconsistent to measure the water adsorption capacity of the sorbent. Thus, it is not recommended to use it for future measurements. The data obtained from the breakthrough method in this work is not to be trusted, and previously published data from Veneman et al.[1] is thought to be subject to the same problems. Instead, a new measurement method based on gravimetric measurements was developed in this work, as described in subsection 3.3. It was proven to work consistently and precise enough to obtain the required data.

Experimental results of gravimetric experiments show that the studied sorbent (Lewatit VP OC 1065<sup>TM</sup>) is Type V and heterogeneous. The interaction between Lewatit and water is energetically weak, and the BET model is not applicable to this type of sorbent. The AD-Toth isotherm model describes the sorbent behavior at ambient temperature throughout the entire range of RH best, but the GAB model was selected over it due to its theoretical significance.

The temperature-dependent GAB isotherm model is the main output of this research. It describes the system well at the relevant ranges of relative humidity (5-85%) and temperature (5-35°C). The adsorption heat of water over Lewatit was estimated to be on the range of  $\Delta H_{ads,w} = (63 - 50) kJ/mol$ .

The hysteresis loop is outstandingly wide, with hysteresis present in the entire range studied (7-93%). This has important implications for real DAC operation. Quick drops in the ambient relative humidity due to weather changes may require stopping the cycle prematurely at certain conditions.

Analysis of the energy requirements based on the new experimental data suggest that operation is the least energy intensive in dry conditions, even when accounting for the enhancement of  $q_{CO_2,eq}$  in the presence of water. The optimum adsorption temperature depends on the regeneration method. Mild temperatures are generally better for N<sub>2</sub> regeneration while low temperatures are best for steam regeneration.

### 5.2 Recommendations

For future experiments on the topic of measuring equilibrium capacities of water, it is recommended to use the experimental method described at the end of subsection 4.2. However, if a future researcher instead decides to use the gravimetric method developed in this work, various improvements are recommended:

- It would be important to perform experiments to check the accuracy of the method by using a sorbent of known adsorption capacity.
- The precision of the method should be characterized by performing several single equilibrium experiments at a specific value of RH and temperature to estimate the standard deviation of the method.
- It would be best if the flask used in the experiments did not change its weight with temperature or in contact with water, for improved blank measurements.
- It is recommended to measure the humidity at the outlet of the humidifier instead of in the gas feed to be able to perform capacity measurements in the low RH range and reduce measurement uncertainty.
- In order to be able to measure capacities at higher temperatures than the ones presented here, two things would be required: connecting a water bath to the humidifier walls to reach higher water pressures, and install steel piping with heat tracing from the humidifier outlet to the setup inlet to avoid condensation.

For the reasons described in subsection 4.3.2, the temperature dependent isotherm model is somewhat lacking. The main reason is that it is based only on two data sets of temperature, and thus some of its implications are unclear. More research of equilibrium capacities at different temperatures is needed to expand on it and improve it, due to its major relevance for the design of a sorbent-based DAC process.

Experimental results show that the hysteresis loop of the system is extremely wide. This is a surprising result difficult to reconcile with previous literature. More research is needed to understand the pore structure of Lewatit and its unexplained hysteresis behavior, for example by performing mercury porosimetry measurements. In addition, it is recommended to study different hysteresis cycles experimentally to characterize the possible effect on the adsorption step of a DAC process.

## References

- [1] R. Veneman, N. Frigka, W. Zhao, Z. Li, S. Kersten, and W. Brilman, "Adsorption of h<sub>2</sub>o and co<sub>2</sub> on supported amine sorbents," *International journal of greenhouse gas control*, vol. 41, pp. 268–275, 2015.
- [2] F. Mackenzie, A. Lerman, and A. Andersson, "Past and present of sediment and carbon biogeochemical cycling models," *Biogeosciences Discussions*, vol. 1, no. 1, pp. 27–85, 2004.
- [3] N. Aeronautics and S. A. (NASA). (2019) Effects of climate change. [Online]. Available: <https://climate.nasa.gov/effects/>
- [4] V. Smil, *The Earth's biosphere: Evolution, dynamics, and change*. Mit Press, 2003.
- [5] U. S. E. P. A. (EPA). (2018) Overview of greenhouse gases. [Online]. Available: <https://www.epa.gov/ghgemissions/overview-greenhouse-gases>
- [6] R. K. Pachauri, M. R. Allen, V. R. Barros, J. Broome, W. Cramer, R. Christ, J. A. Church, L. Clarke, Q. Dahe, P. Dasgupta *et al.*, *Climate change 2014: synthesis report. Contribution of Working Groups I, II and III to the fifth assessment report of the Intergovernmental Panel on Climate Change*. IPCC, 2014.
- [7] N. G. M. D. (GMD). (2019) Trends in atmospheric carbon dioxide. [Online]. Available: [https://www.esrl.noaa.gov/gmd/ccgg/trends/gl\\_trend.html](https://www.esrl.noaa.gov/gmd/ccgg/trends/gl_trend.html)
- [8] "Adoption of the paris agreement," 2015.
- [9] I. C. Change, "The physical science basis. contribution of working group 1 to the fifth assessment report of the intergovernmental panel on climate change. 2013," pp. 33–118, 2013.
- [10] U. E. I. A. (EIA). (2019) International energy outlook 2018. [Online]. Available: <https://www.eia.gov/outlooks/ieo/>
- [11] E. E. S. Michaelides, *Alternative energy sources*. Springer Science & Business Media, 2012.
- [12] S. J. Davis, N. S. Lewis, M. Shaner, S. Aggarwal, D. Arent, I. L. Azevedo, S. M. Benson, T. Bradley, J. Brouwer, Y.-M. Chiang *et al.*, "Net-zero emissions energy systems," *Science*, vol. 360, no. 6396, p. eaas9793, 2018.
- [13] D. McLaren, "A comparative global assessment of potential negative emissions technologies," *Process Safety and Environmental Protection*, vol. 90, no. 6, pp. 489–500, 2012.
- [14] L. R. Boysen, W. Lucht, D. Gerten, V. Heck, T. M. Lenton, and H. J. Schellnhuber, "The limits to global-warming mitigation by terrestrial carbon removal," *Earth's Future*, vol. 5, no. 5, pp. 463–474, 2017.
- [15] E. S. Sanz-Perez, C. R. Murdock, S. A. Didas, and C. W. Jones, "Direct capture of co<sub>2</sub> from ambient air," *Chemical reviews*, vol. 116, no. 19, pp. 11 840–11 876, 2016.
- [16] J. Wohland, D. Witthaut, and C.-F. Schleussner, "Negative emission potential of direct air capture powered by renewable excess electricity in europe," *Earth's Future*, vol. 6, no. 10, pp. 1380–1384, 2018.
- [17] M. Bui, C. S. Adjiman, A. Bardow, E. J. Anthony, A. Boston, S. Brown, P. S. Fennell, S. Fuss, A. Galindo, L. A. Hackett *et al.*, "Carbon capture and storage (ccs): the way forward," *Energy & Environmental Science*, vol. 11, no. 5, pp. 1062–1176, 2018.
- [18] K. Lackner, H.-J. Ziock, and P. Grimes, "Carbon dioxide extraction from air: Is it an option?" Los Alamos National Lab., NM (US), Tech. Rep., 1999.
- [19] R. Veneman, "Adsorptive systems for post-combustion co<sub>2</sub> capture: design, experimental validation and evaluation of a supported amine based process," 2015.
- [20] M. Bos, S. Pietersen, and D. Brilman, "Production of high purity co<sub>2</sub> from air using solid amine sorbents," *Chemical Engineering Science*, 2019.
- [21] M. Mukhopadhyay, *Fundamentals of cryogenic engineering*. PHI Learning Pvt. Ltd., 2010.
- [22] M. Fasihi, O. Efimova, and C. Breyer, "Techno-economic assessment of co<sub>2</sub> direct air capture plants," *Journal of cleaner production*, vol. 224, pp. 957–980, 2019.
- [23] M. J. Bos, T. Kreuger, S. Kersten, and D. Brilman, "Study on transport phenomena and intrinsic kinetics for co<sub>2</sub> adsorption in solid amine sorbent," *Chemical Engineering Journal*, 2018.

- [24] D. D. Do *et al.*, *Adsorption analysis: equilibria and kinetics*. Imperial college press London, 1998, vol. 2.
- [25] Q. Yu, "Direct capture of co<sub>2</sub> from ambient air using solid sorbents," Ph.D. dissertation, University of Twente, 2018.
- [26] M. Donohue and G. Aranovich, "Classification of gibbs adsorption isotherms," *Advances in Colloid and Interface Science*, vol. 76, pp. 137–152, 1998.
- [27] I. Portugal, V. M. Dias, R. F. Duarte, and D. V. Evtuguin, "Hydration of cellulose/silica hybrids assessed by sorption isotherms," *The Journal of Physical Chemistry B*, vol. 114, no. 11, pp. 4047–4055, 2010.
- [28] E. O. Timmermann, "Multilayer sorption parameters: Bet or gab values?" *Colloids and Surfaces A: Physicochemical and Engineering Aspects*, vol. 220, no. 1-3, pp. 235–260, 2003.
- [29] E. J. Quirijns, A. J. Van Boxtel, W. K. van Loon, and G. Van Straten, "Sorption isotherms, gab parameters and isosteric heat of sorption," *Journal of the Science of Food and Agriculture*, vol. 85, no. 11, pp. 1805–1814, 2005.
- [30] M. Monleón Pradas, M. Salmerón Sánchez, G. Gallego Ferrer, and J. L. Gómez Ribelles, "Thermodynamics and statistical mechanics of multilayer adsorption," *The Journal of chemical physics*, vol. 121, no. 17, pp. 8524–8531, 2004.
- [31] G. L. Aranovich and M. D. Donohue, "A new approach to analysis of multilayer adsorption," *Journal of colloid and interface science*, vol. 173, no. 2, pp. 515–520, 1995.
- [32] K.-M. Kim, H.-T. Oh, S.-J. Lim, K. Ho, Y. Park, and C.-H. Lee, "Adsorption equilibria of water vapor on zeolite 3a, zeolite 13x, and dealuminated y zeolite," *Journal of Chemical & Engineering Data*, vol. 61, no. 4, pp. 1547–1554, 2016.
- [33] N. Ayawei, A. N. Ebelegi, and D. Wankasi, "Modelling and interpretation of adsorption isotherms," *Journal of Chemistry*, vol. 2017, 2017.
- [34] J. Rouquerol, F. Rouquerol, P. Llewellyn, G. Maurin, and K. S. Sing, *Adsorption by powders and porous solids: principles, methodology and applications*. Academic press, 2013.
- [35] S. Li, S. Deng, L. Zhao, R. Zhao, M. Lin, Y. Du, and Y. Lian, "Mathematical modeling and numerical investigation of carbon capture by adsorption: Literature review and case study," *Applied Energy*, vol. 221, pp. 437–449, 2018.
- [36] "Product and manufacturer information - lewattit vp oc 1065," 2011.
- [37] M. B. Ravazio, "The synthesis of an amine-based sorbent for capturing atmospheric co<sub>2</sub>," 2019.
- [38] Q. Yu, J. d. l. P. Delgado, R. Veneman, and D. W. Brilman, "Stability of a benzyl amine based co<sub>2</sub> capture adsorbent in view of regeneration strategies," *Industrial & engineering chemistry research*, vol. 56, no. 12, pp. 3259–3269, 2017.
- [39] W. R. Alesi Jr and J. R. Kitchin, "Evaluation of a primary amine-functionalized ion-exchange resin for co<sub>2</sub> capture," *Industrial & Engineering Chemistry Research*, vol. 51, no. 19, pp. 6907–6915, 2012.
- [40] M. Parvazinia, S. Garcia, and M. Maroto-Valer, "Co<sub>2</sub> capture by ion exchange resins as amine functionalised adsorbents," *Chemical Engineering Journal*, vol. 331, pp. 335–342, 2018.
- [41] A. L. Buck, "New equations for computing vapor pressure and enhancement factor," *Journal of applied meteorology*, vol. 20, no. 12, pp. 1527–1532, 1981.
- [42] N. Frigka, "Experimental study of co<sub>2</sub> and h<sub>2</sub>o adsorption," 2014.
- [43] M. Belhocine, A. Haouzi, G. Bassou, T. Phou, D. Maurin, J.-L. Bantignies, and F. Henn, "Isosteric heat of water adsorption and desorption in homoionic alkaline-earth montmorillonites," *Chemical Physics*, vol. 501, pp. 26–34, 2018.
- [44] A. Haque, N. Shimizu, T. Kimura, and B. Bala, "Net isosteric heats of adsorption and desorption for different forms of hybrid rice," *International Journal of Food Properties*, vol. 10, no. 1, pp. 25–37, 2007.
- [45] T. van Schagen, "Dynamic modelling and optimization of an adsorption based dac system," 2019.
- [46] J. A. Wurzbacher, C. Gebald, S. Brunner, and A. Steinfeld, "Heat and mass transfer of temperature–vacuum swing desorption for co<sub>2</sub> capture from air," *Chemical Engineering Journal*, vol. 283, pp. 1329–1338, 2016.

- [47] D. R. Holycross and M. Chai, "Comprehensive nmr studies of the structures and properties of pei polymers," *Macromolecules*, vol. 46, no. 17, pp. 6891–6897, 2013.
- [48] S. R. Batten, N. R. Champness, X.-M. Chen, J. Garcia-Martinez, S. Kitagawa, L. Öhrström, M. O’Keeffe, M. P. Suh, and J. Reedijk, "Coordination polymers, metal–organic frameworks and the need for terminology guidelines," *CrystEngComm*, vol. 14, no. 9, pp. 3001–3004, 2012.
- [49] Y. G. Ko, S. S. Shin, and U. S. Choi, "Primary, secondary, and tertiary amines for co<sub>2</sub> capture: Designing for mesoporous co<sub>2</sub> adsorbents," *Journal of colloid and interface science*, vol. 361, no. 2, pp. 594–602, 2011.
- [50] J. Yu and S. S. Chuang, "The role of water in co<sub>2</sub> capture by amine," *Industrial & Engineering Chemistry Research*, vol. 56, no. 21, pp. 6337–6347, 2017.
- [51] S. A. Didas, M. A. Sakwa-Novak, G. S. Foo, C. Sievers, and C. W. Jones, "Effect of amine surface coverage on the co-adsorption of co<sub>2</sub> and water: spectral deconvolution of adsorbed species," *The journal of physical chemistry letters*, vol. 5, no. 23, pp. 4194–4200, 2014.
- [52] W. Buijs and S. de Flart, "Direct air capture of co<sub>2</sub> with an amine resin: A molecular modeling study of the co<sub>2</sub> capturing process," *Industrial & engineering chemistry research*, vol. 56, no. 43, pp. 12 297–12 304, 2017.
- [53] K. Li, J. D. Kress, and D. S. Mebane, "The mechanism of co<sub>2</sub> adsorption under dry and humid conditions in mesoporous silica-supported amine sorbents," *The Journal of Physical Chemistry C*, vol. 120, no. 41, pp. 23 683–23 691, 2016.
- [54] C.-H. Chen, D. Shimon, J. J. Lee, F. Mentink-Vigier, I. Hung, C. Sievers, C. W. Jones, and S. E. Hayes, "The "missing" bicarbonate in co<sub>2</sub> chemisorption reactions on solid amine sorbents," *Journal of the American Chemical Society*, vol. 140, no. 28, pp. 8648–8651, 2018.
- [55] O. Akingbogun, L. Muhr, and C. Vallieres, "Capture of carbon dioxide by an ion-exchange resin: Influence of gas humidity on capture mechanisms," *Separation Science and Technology*, vol. 52, no. 10, pp. 1761–1767, 2017.
- [56] M. W. Hahn, M. Steib, A. Jentys, and J. A. Lercher, "Mechanism and kinetics of co<sub>2</sub> adsorption on surface bonded amines," *The Journal of Physical Chemistry C*, vol. 119, no. 8, pp. 4126–4135, 2015.

## List of Symbols

| Symbol           | Units (SI convention)               | Description                                    |
|------------------|-------------------------------------|--|
| $R$              | $\text{m}^3\text{Pa}/(\text{molK})$ | Ideal gas constant                             |
| $T$              | K                                   | Temperature                                    |
| $p$              | Pa                                  | Partial pressure                               |
| $P$              | Pa                                  | Total pressure                                 |
| $p^{sat}$        | Pa                                  | Saturation pressure                            |
| $t$              | s                                   | Time   |
| $q$              | $\text{mol}/\text{kg}$              | Adsorption capacity                            |
| $q_m$            | $\text{mol}/\text{kg}$              | Monolayer adsorption capacity                  |
| $\xi$            | -                                   | Degree of monolayer occupation                 |
| $H$              | J/mol                               | Enthalpy                                       |
| $\Delta H_{ads}$ | J/mol                               | Heat of adsorption                             |
| $\Delta H_{vap}$ | J/mol                               | Heat of vaporization                           |
| $\Delta H_{is}$  | J/mol                               | Isosteric heat of adsorption                   |
| $b$              | 1/Pa                                | Adsorption equilibrium constant                |
| $d$              | -                                   | Aranovich-Donohue isotherm divergence constant |
| $n$              | -                                   | Sips isotherm constant                         |
| $th$             | -                                   | Toth isotherm constant                         |
| $C$              | -                                   | GAB isotherm constants                         |
| $k$              | -                                   | GAB isotherm constants                         |
| $\Delta H_C$     | J/mol                               |  |
| $\Delta H_k$     | J/mol                               |  |
| $C_0$            | -                                   | Temperature dependent GAB model parameters     |
| $k_0$            | -                                   |  |
| $q_{m,0}$        | $\text{mol}/\text{kg}$              |  |
| $\beta$          | K                                   |  |
| $R^2$            | -                                   | Coefficient of determination                   |
| $r_K$            | m                                   | Kelvin radius                                  |
| $V_M$            | $\text{mol}/\text{m}^3$             | Molar volume                                   |
| $\sigma$         | N/m                                 | Surface tension                                |
| $\theta$         | rad                                 | Meniscus angle                                 |
| $N$              | $\text{mol}/\text{s}$               | Molar flowrate                                 |
| $X$              | -                                   | Mole fraction                                  |
| $RH$             | %                                   | Relative humidity                              |
| $m$              | kg                                  | Mass   |
| $MW$             | $\text{kg}/\text{mol}$              | Molecular Weight                               |
| $\phi_V$         | $\text{m}^3/\text{s}$               | Volumetric flowrate                            |
| $\Delta q$       | $\text{mol}/\text{kg}$              | Working capacity of the cycle                  |
| $C_p$            | J/(kgK)                             | Specific heat                                  |
| $Q$              | J/kg CO <sub>2</sub>                | Heat duty per unit of CO <sub>2</sub> captured |
| $\rho$           | $\text{kg}/\text{m}^3$              | Density  |

## A Appendices

### A.1 Review of supported sorbents for CO<sub>2</sub> adsorption

This review is largely based on the work of Sanz et al. [15]. The most important solid-supported adsorbents for CO<sub>2</sub> capture include metal oxide supported amine sorbents, organic supported amine sorbents and metal organic frameworks.

In the case of physisorption, pore diameter becomes a key parameter for CO<sub>2</sub> uptake if the material is microporous. Mesoporous materials, which are often employed for this reason, have much larger pore diameters making containment effects less relevant. Gas-surface interaction and surface area correlate with CO<sub>2</sub> uptake, but if amines are present in the material it is mainly determined by the amine loading. This is even more so at lower CO<sub>2</sub> concentrations (under 1%), which is the range that concerns this work. Thus, amine-based sorbents are the most common solid-supported adsorbents used in DAC research [15].

Metal oxide supported amine adsorbents are divided in three classes. Class 1 adsorbents incorporate polyamine structures physically impregnated within the pores of the support. Class 2 adsorbents contain single amine moieties covalently bonded to the support walls. Class 3 adsorbents contain polyamine structures covalently bonded to the support walls. A combination of classes 1 and 2 is also possible, where amines can be found both tethered to the support and physically impregnated over the walls [15].

#### A.1.1 Metal oxide supported amine sorbents

Poly(ethylenimine) (PEI) has been largely studied due to its large density of amine groups combined with good stability under Temperature Swing Adsorption (TSA) and Vacuum Swing Adsorption (VSA). It could be considered as the benchmark for class 1 materials and amine sorbents in general. Secondary amines are generally regarded as the best compromise between reactivity (where primary amines excel) and heat of adsorption (where tertiary amines excel). In general, branched PEI over a silica support is considered the best known option in this class, providing a balance between capacity and kinetics. It contains primary, secondary, and tertiary amine groups in varying ratios between 1:1:1 and 1:2:1 [47], and a CO<sub>2</sub> uptake of up to 2.44 mol of CO<sub>2</sub> per kg of sorbent at DAC conditions. The temperature swing required for these type of materials may be very small on the range of 50-60 °C [15]. However, due to the relatively weak nature of the amine-support interaction, these materials are often subject to noticeable amine loss due to evaporation at desorption temperatures [19].

Class 2 and 3 metal oxide amine sorbents comprise materials composed of amines covalently bonded to metal oxide supports. Primary amines have been proven superior compared to the others in class 2 sorbents at DAC conditions, and lower CO<sub>2</sub> uptakes and cyclic stability compared to class 1 sorbents have been found so far [15]. Class 3 sorbents have shown improved results in both aspects comparable to class 1 sorbents, and currently hold the record for flue gas CO<sub>2</sub> capture at 11.8 mol/kg. More research on the field of DAC is needed on these promising sorbents. The influence of Relative Humidity (RH) of the feed on the DAC CO<sub>2</sub> uptake shows no clear general trends for porous oxide supported sorbents, being beneficial in many cases and inconsequential or detrimental in others [15].

#### A.1.2 Organic solid supported amine sorbents

Organic solid supported amine sorbents have been extensively researched as well. These materials have been under commercial use for years, such as CO<sub>2</sub> scrubbing in submarines and other confined spaces or creation of CO<sub>2</sub> rich atmospheres in greenhouses. These can also be distinguished depending on whether the amine active phase is impregnated or covalently bonded to the support. Of particular interest for DAC are amine-based anion exchange resins, which after PEI impregnation have reached remarkable CO<sub>2</sub> uptakes of up to 2.26 mol/kg. In general, organic-based sorbents have shown important increments on CO<sub>2</sub> uptake with increasing relative humidity under DAC conditions. Some authors suggest that this may be related to the slow diffusion of ultradilute CO<sub>2</sub> across the sorbent bulk. Water would yield diffusive intermediates which enhance the mobility of CO<sub>2</sub> towards the active sites. This is consistent with studies on flue gas in which moisture yields faster CO<sub>2</sub> uptake and diffusion [15].

### A.1.3 Metal organic frameworks

Metal Organic Frameworks (MOFs) are highly ordered materials composed of networks of metal atoms or clusters coordinated to organic ligands forming open one-, two-, or three-dimensional structures containing potential voids [48]. Being physisorbents, they have a lower heat of adsorption and thus require less energy for regeneration. They have a high degree of tunability by allowing modification of pore size and incorporation of additional reactivity. By themselves they have poorer CO<sub>2</sub> uptakes and stability than amine sorbents, but they can be improved by amine tethering, leading to exceptionally high uptakes at DAC conditions up to a maximum of 2.83 mol/kg (EN-Mg<sub>2</sub>(dobpdc)) and making them more stable. However, the very limited amount of data available still casts doubt on the commercial viability of these high-potential materials and more research is needed [15].

### A.1.4 Material Selection

While class 2 and 3 metal oxide supported amine sorbents and MOFs are promising materials, more fundamental research is still required to uncover their actual potential for DAC. Thus, they have not been considered as a suitable material for this work.

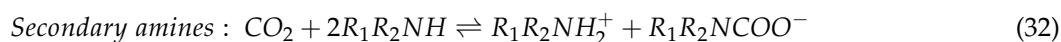
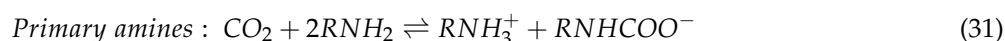
The material selection here is based on the work of Qian Yu [25]. She compared a host of different sorbents, with an emphasis on two amine-functionalized sorbents with good results in terms of CO<sub>2</sub> capacity and selectivity over water, both of them based on an organic divinyl-benzene (DVB) anionic exchange resin support. The first is PEI 600, in which the active phase is comprised of impregnated PEI with an average molecular weight of 600 g/mol over a commercial DVB support. The second is Lewatit VP OC 1065, a commercial sorbent in which the active phase is comprised of primary amine groups covalently bonded to the DVB support. Of these, Lewatit proved to work better in terms of selectivity, thus adsorbing similar amounts of CO<sub>2</sub> but less water. Lewatit was then compared to an analogous material with secondary instead of primary amines, demonstrating a CO<sub>2</sub> capacity over 6 times higher than the alternative. It was found to have a relatively high average CO<sub>2</sub> capacity at about 1.4 mol/kg and a selectivity of CO<sub>2</sub> over H<sub>2</sub>O of approximately 4:1. Additionally, it is resistant to CO<sub>2</sub>-induced degradation at temperatures up to 120 °C and has a stable CO<sub>2</sub> capacity during 18 adsorption cycles [25] and 280 Thermogravimetric Analysis (TGA) cycles [40].

In conclusion, Lewatit VP OC 1065 was selected due to its reasonably good CO<sub>2</sub> capacity at ambient conditions, adequate stability at regeneration conditions, high cyclic stability and scale-up feasibility due to its commercial availability.

## A.2 CO<sub>2</sub> adsorption mechanism

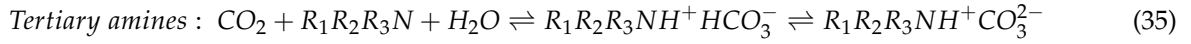
### A.2.1 Possible mechanisms

The mechanism of the reaction can depend on the presence of water. In absence of water, the zwitterionic mechanism takes place. One of the two amine groups involved adopts a proton from the other becoming the positive zwitterionic form, while the other incorporates the CO<sub>2</sub>. It requires two primary or secondary amine moieties to form an ammonium carbamate, as shown in Equation 31 and Equation 32. This means that the maximum ratio of CO<sub>2</sub> captured per amine group is 0.5 (2:1 stoichiometry). The fraction of this value due to amine chemisorption that an amine sorbent can reach in dry conditions is known as the amine efficiency. A value higher than 0.5 is possible, but only if the contribution due to physisorption from the support is also included in the calculation [15].



In the presence of water in the reaction medium, the bicarbonate mechanism can take place instead of the carbamate mechanism. The reaction occurs when water takes part in the reaction, yielding ammonium carbonate or bicarbonate, as shown in Equations (34) to (35). Note that the bicarbonate or carbonate is formed depending on the pH. Secondary and tertiary amines have been shown to undergo this process, while primary amines have not. Furthermore, this is the only known chemical interaction between tertiary amines and CO<sub>2</sub>. Only one amine

moiety is then required to react with a CO<sub>2</sub> molecule, so the maximum CO<sub>2</sub>/amine ratio in humid conditions is then 1.0 (1:1 stoichiometry) [15].



### A.2.2 Mechanism in Lewatit

The zwitterionic mechanism for CO<sub>2</sub> adsorption for primary amine sorbents presented in Equation 31 was proven to take place in liquid amine sorbents [49]. It is also considered to be the most likely mechanism in primary amine sorbents [25, 50, 51], including Lewatit [25, 52]. The adsorption mechanism of secondary and tertiary amines is not discussed further, since virtually only primary amines can be found in Lewatit.

The zwitterionic mechanism (Equation 31) is predicted to be more favored than the bicarbonate mechanism (Equation 33) in primary amines based on quantum chemical calculations for amine-impregnated sorbents. Results showed that the zwitterion can be stabilized by water as well as amines, making it serve as a diffusional intermediate for CO<sub>2</sub> transport [53]. Simulations predict that direct amine-H<sub>2</sub>O catalyzed formation of carbamic acid is the most likely mechanism for CO<sub>2</sub> capture in Lewatit [52]. Amine-amine catalyzed formation of carbamic acid was also found to be somewhat favored, and was thus proposed as the most likely mechanism in dry conditions. However, since there is conclusive proof of some presence of bicarbonate in humid conditions for primary amine sorbents (specially at low amine loading) [51, 54], the exact mechanism is still disputed.

Because the two mechanisms have different amine efficiency, researchers have turned to the stoichiometry of their measurements over Lewatit, reaching disparate conclusions about the mechanism [52, 55]. Initially, it would seem that the apparent 2:1 stoichiometry favors the zwitterionic explanation (based on a 6.7 mol/kg of amine loading and a theoretical capacity of 3.37 mol/kg). However, as explained in subsection 3.1, it is possible that up to half the amine sites in Lewatit are unreachable, as shown by titration measurements. In this case, there would be a 1:1 stoichiometry which could be explained by the bicarbonate mechanism. The site availability directly affects any conclusion based on stoichiometry, so without reconciling these two one cannot ascertain the mechanism.

Some researchers have proposed that in amine-impregnated sorbents the presence of water causes the mechanism to switch from the zwitterionic mechanism to the formation of bicarbonate, thus increasing the maximum CO<sub>2</sub> uptake [56]. This would be in accordance with the detection of bicarbonate in related systems [51, 54]. It is possible that this phenomenon takes place in Lewatit, since the CO<sub>2</sub> uptake does go up with the relative humidity. Still, other explanations are also possible such as a beneficial physical interaction between CO<sub>2</sub> and H<sub>2</sub>O or shielding of amine sites by H<sub>2</sub>O [1].

In summary, the adsorption mechanism requires further research for elucidation. Studies that clarify the site availability of Lewatit could be particularly enlightening. However, if we assume that half of the amine sites are unavailable for reaction as the titration measurements seem to suggest, the bicarbonate mechanism seems like the most plausible explanation.

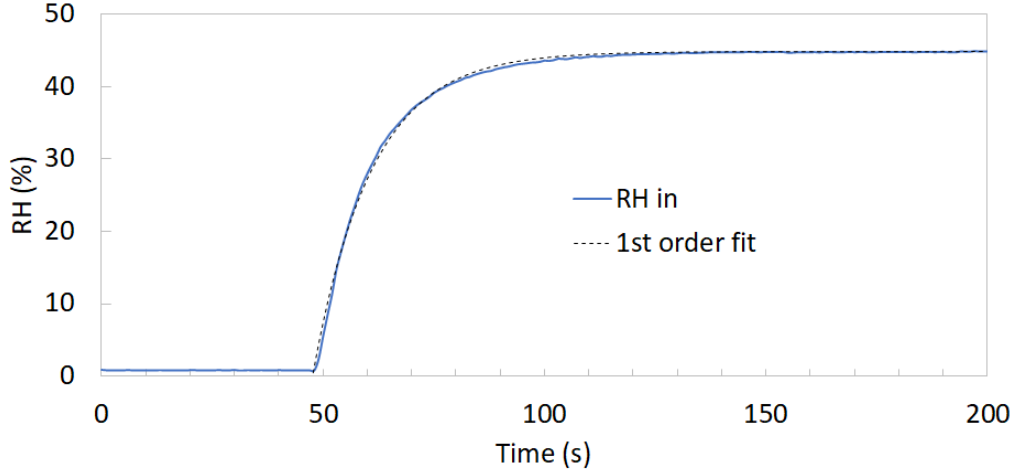
### A.3 Response time deconvolution analysis

The response time of the sensors was fitted to a first order response time function (Equation 36) successfully, as shown in Figure 36. The response time constant  $\tau$  was calculated using the value of RH at 63%, 95% and 99% of the total RH response. It was different for each of the two sensors, the outlet one being slower than the inlet one. The values of the time constant  $\tau$  were fairly consistent for different values of flowrate and humidity, and independent of the position of the sensor. The values of the constants for the response to ambient conditions are found in Table 6.

$$y(t) = y_0 + k_t(1 - e^{-(t-t_0)/\tau}) \quad (36)$$

**Table 6:** Response time constants for the response to ambient conditions.

|               | $k_t$ | $\tau$ | $y_0$ |
|---------------|-------|--------|-------|
| Inlet sensor  | 44,0  | 13,2   | 0,86  |
| Outlet sensor | 42,1  | 24,6   | 0,86  |


**Figure 36:** Fit of the sensor response to ambient conditions to a first order response time function.

In order to perform deconvolution of the RH signal of the sensors, the Fourier transform of the response time fitted function was computed to obtain the transfer function. Let  $s_t$  be the first derivative of the response of the sensor:

$$s_t = y(t)(1 - e^{-(t/\tau)}) \quad (37)$$

$$s_{t+1} = s_t + \frac{ds}{dt} \Delta t \quad (38)$$

It was found that  $ds/dt$  can be calculated as a Taylor series whose infinite sum approximates to a convergent series that converges to the following expression for  $|\tau| > 1$  and  $t \in \mathbb{R}$ :

$$\frac{ds}{dt} = \sum_{n=1}^{\infty} \left( \frac{e^{(-t/\tau)}}{\tau^n} \right) * (-1)^{-n} = t \frac{e^{-t/\tau}}{\tau + 1} \quad (39)$$

Thus, the deconvolved RH signal can be obtained by:

$$y(t) = \frac{s_{t+1}}{1 + e^{-t/\tau} (1/\tau - 1) \Delta t} \quad (40)$$

Applying the deconvolution to an example set of experimental data results in the values shown in Figure 37.

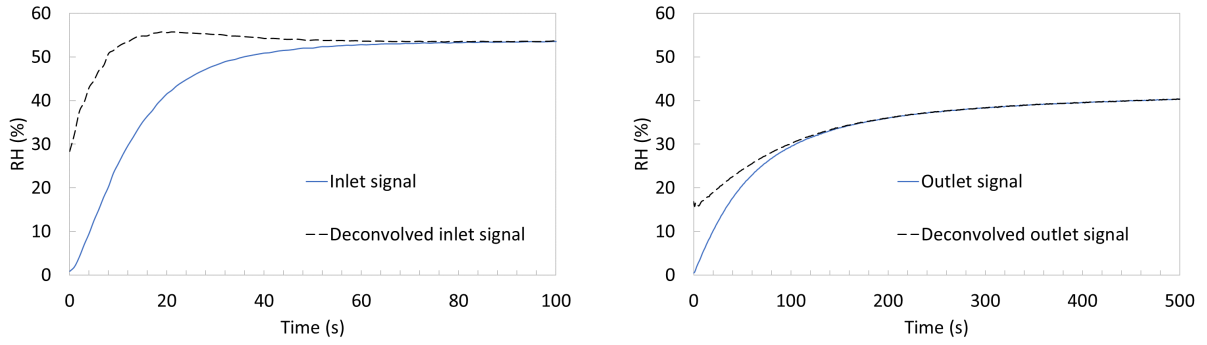


Figure 37: Deconvolved RH signal for inlet and outlet measurements of an example experiment.

#### A.4 Process design parameters

Table 7: Physical properties.

|                       |       |          |
|-----------------------|-------|----------|
| $\Delta H_{ads,CO_2}$ | 75    | kJ/mol   |
| $\Delta H_{vap,H_2O}$ | 43    | kJ/mol   |
| $MW_{CO_2}$           | 44.01 | g/mol    |
| $MW_{H_2O}$           | 18.02 | g/mol    |
| $MW_{air}$            | 28.96 | g/mol    |
| $Cp_{steam}$          | 1909  | J/(kg·K) |
| $Cp_{water}$          | 4180  | J/(kg·K) |
| $Cp_{sorbent}$        | 1580  | J/(kg·K) |
| $Cp_{air}$            | 1007  | J/(kg·K) |
| $Cp_{N_2}$            | 1023  | J/(kg·K) |

Table 8: Model inputs, unless otherwise stated.

|   |        |        |
|---|--------|--------|
| $\phi_{v,desorption}$ (steam)           | 1      | NL/min |
| $T_{regeneration}$ (steam)              | 120    | °C     |
| $\phi_{v,desorption}$ (N <sub>2</sub> ) | 20     | NL/min |
| $T_{regeneration}$ (N <sub>2</sub> )    | 90     | °C     |
| $t_{desorption}$                        | 1.5    | h      |
| $P_{desorption}$                        | 101300 | Pa     |
| $mCp(reactor) / mCp(sorbent)$           | 1      |        |
| $m_{sorbent}$                           | 1.6    | kg     |

### A.5 Sensitivity analysis of energy requirements

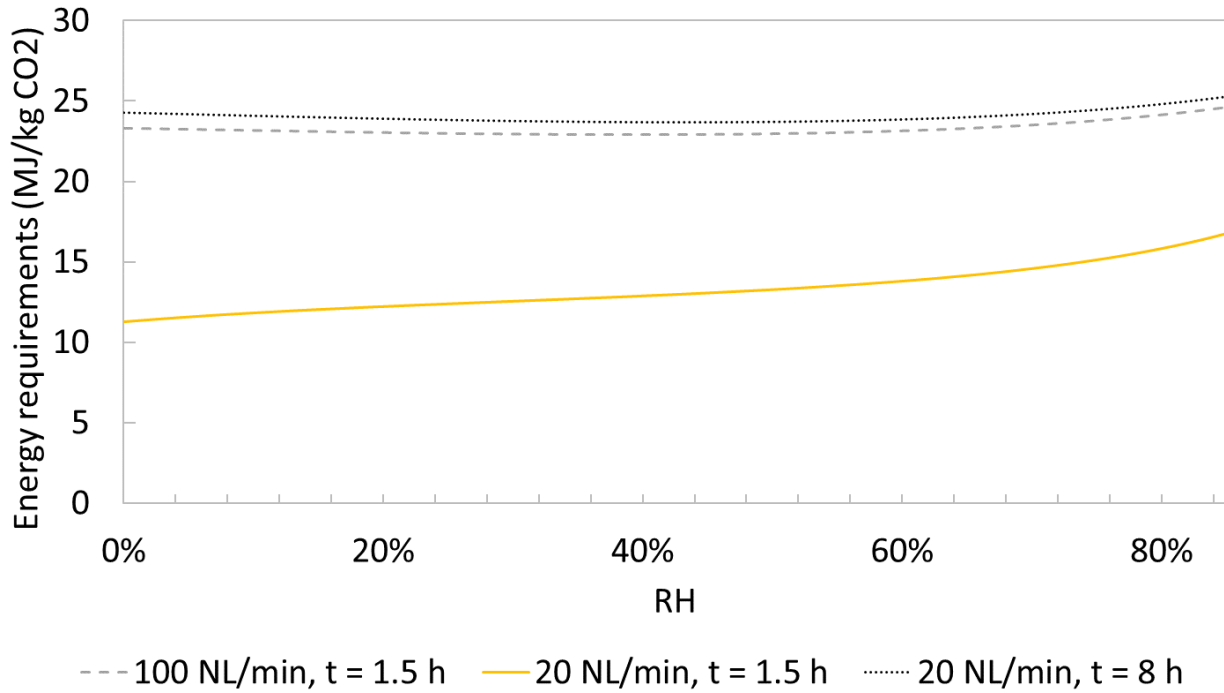


Figure 38: Sensitivity analysis of energy requirements of the DAC cycle for N<sub>2</sub> regeneration at different values of purge gas flowrate and desorption time.

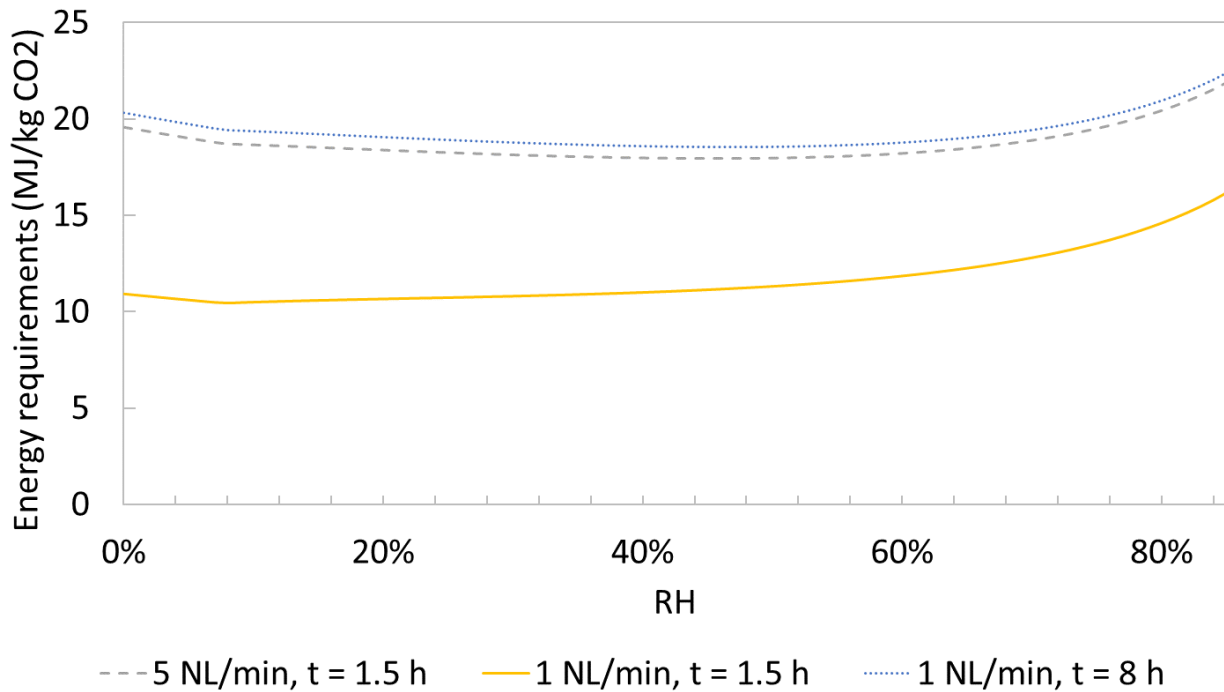


Figure 39: Sensitivity analysis of energy requirements of the DAC cycle for steam regeneration at different values of purge gas flowrate and desorption time.

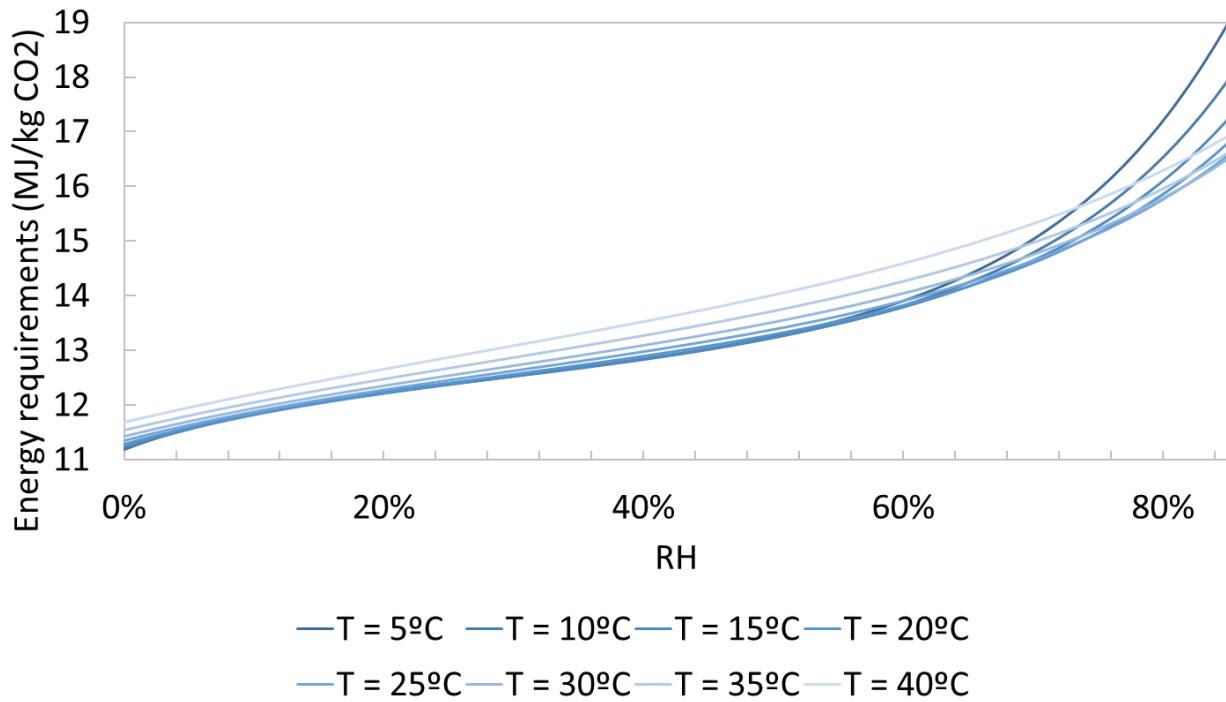


Figure 40: Sensitivity analysis of energy requirements of the DAC cycle for N<sub>2</sub> regeneration at different adsorption step temperatures.

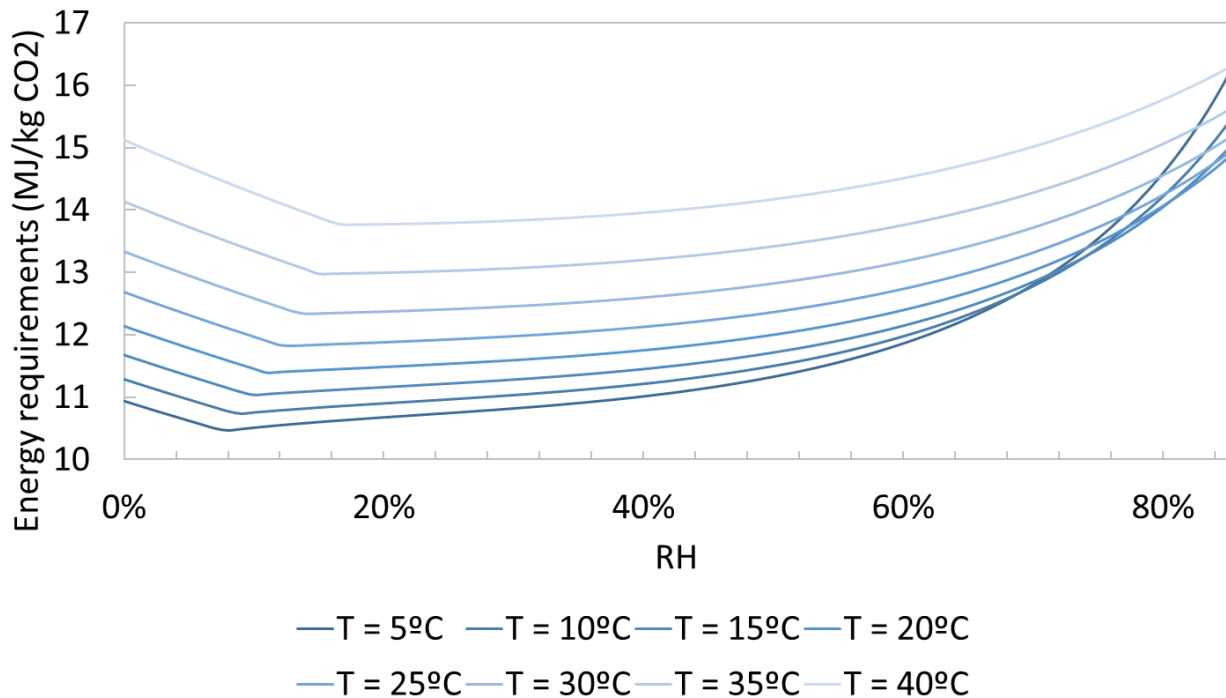
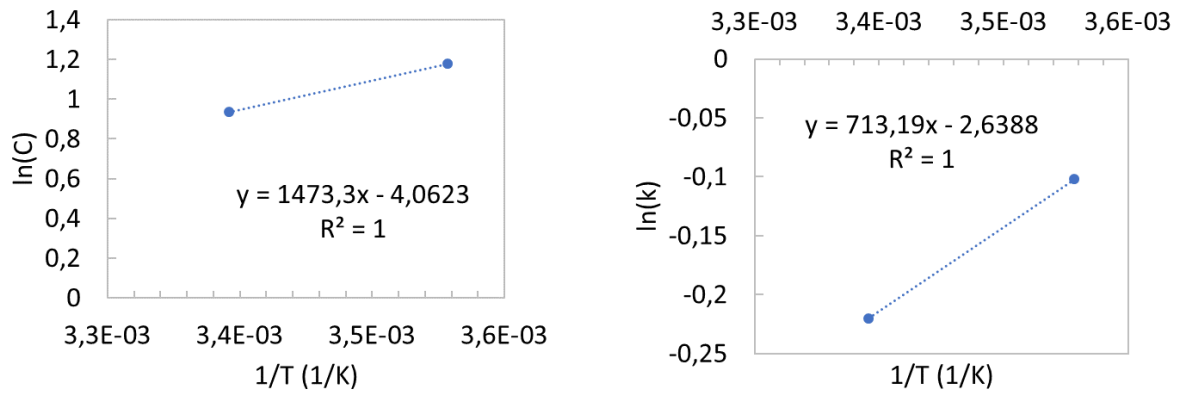


Figure 41: Sensitivity analysis of energy requirements of the DAC cycle for steam regeneration at different adsorption step temperatures.

### A.6 Temperature dependent model parameter regression



**Figure 42:** Two-point linear regression of the C and k parameters of the temperature dependent GAB isotherm model to obtain the parameters  $\Delta H_C$  and  $\Delta H_k$ .

## List of Figures

|    |  |    |
|----|--|----|
| 1  | Global mean surface temperature increase as a function of cumulative total global CO <sub>2</sub> emissions, together with model predictions for different scenarios. For more information, see AR5 Climate Change: The Physical Science Basis [9]. . . . .                  | 1  |
| 2  | A selection of carbon capture pathways in relation to the carbon cycle. The dashed line represents the boundaries of the cycle at the relevant timescale. . . . .  | 2  |
| 3  | Example of a general low temperature solid sorbent DAC system [22]. (1) May not apply in some systems. . . . .   | 4  |
| 4  | Experimental data of H <sub>2</sub> O equilibrium capacities for Lewatit, without (black symbols) and with (white symbols) CO <sub>2</sub> present, at varying relative humidity [1]. . . . .  | 6  |
| 5  | Isotherm types for mesoporous adsorbents. The curves represent adsorption capacity (Y axis) versus adsorbate activity (X axis). . . . .  | 7  |
| 6  | Enthalpy of water molecules (shaded) at different energy levels represented by GAB enthalpic parameters [29]. . . . .  | 9  |
| 7  | Graphical description of the hysteresis mechanism of pore filling[35]. . . . .   | 10 |
| 8  | IUPAC classification of hysteresis loops[34]. . . . .  | 11 |
| 9  | Representation of a fragment of the PS-DVB polymer backbone of Lewatit VP OC 1065 <sup>TM</sup> . . . . .  | 12 |
| 10 | Constituent monomers of Lewatit VP OC 1065 <sup>TM</sup> . . . . .   | 12 |
| 11 | Process flow diagram of the adsorption-desorption setup. . . . .   | 14 |
| 12 | Data sample from a breakthrough method experiment. Note: the legend in the first graph applies to all graphs in the figure. . . . .  | 15 |
| 13 | Determination of equilibrium point for the breakthrough method. Note: the examples in Figure 13a and Figure 13b are given for two different experiments. . . . .   | 17 |
| 14 | Water adsorption capacity over time before and after correction for the concentration gap. . . . .   | 17 |
| 15 | Examples of raw RH data and calculated capacity over time for single (left) and multiple (right) water breakthrough experiments. . . . .   | 18 |
| 16 | Diagram of the simplified setup. . . . .   | 19 |
| 17 | Water adsorption equilibrium data at 15°C for two different values of flowrate. . . . .  | 20 |
| 18 | Water adsorption equilibrium data at 20°C for varying values of flowrate. . . . .  | 20 |
| 19 | Lewatit and zeolite sorbent particles in the quantity of approximately 1 gram. . . . .   | 21 |
| 20 | Results of water adsorption equilibrium data at different temperatures and constant flowrate using the breakthrough method, together with Veneman's literature data. Note: Veneman's data is not isothermal[1]. . . . .  | 22 |
| 21 | Results of water adsorption equilibrium data at ambient temperature, showing which data points were obtained separately and which were obtained in a multiple equilibrium experiment via the gravimetric method. . . . .   | 23 |
| 22 | Results of water adsorption equilibrium data at different temperatures using the gravimetric method, together with Veneman's literature data. The small graph is a zoom in the region of RH = 30-85%. Note: Veneman's data is not isothermal[1]. . . . .                     | 24 |
| 23 | Theoretical adsorption isotherm model fits of the gravimetric method results at T = 21.7°C. . . . .  | 26 |
| 24 | Semiempirical adsorption isotherm model fits of the gravimetric method results at T = 21.7°C. . . . .  | 27 |
| 25 | Residual plot of the GAB model fit of the data. . . . .  | 28 |
| 26 | Temperature dependent isotherm model and experimental data. . . . .  | 29 |
| 27 | Parity plot of the temperature dependent model within the RH range of validity. . . . .  | 29 |
| 28 | Heat of adsorption of water over Lewatit, enthalpy of vaporization and isosteric heat for different values of adsorption capacity. . . . .   | 30 |
| 29 | Degree of monolayer occupation predicted by the model at different temperatures. . . . .   | 31 |
| 30 | Hysteresis behavior of the system shown by the adsorption equilibrium capacity of water when going forwards and backwards in RH for T = 21.7°C (top) and T = 8°C (bottom). . . . .   | 32 |
| 31 | Kelvin radius of the Lewatit-water system. . . . .   | 33 |
| 32 | Hysteresis behavior of the system at ambient temperature. The dashed lines represent author interpretations of hypothetical hysteresis loops at different values of RH. Note: the AD(Toth) model is used to properly describe the adsorption at the higher RH range. . . . . | 34 |
| 33 | Equilibrium adsorption capacities of water and CO <sub>2</sub> versus relative humidity for the two extremes of the relevant range of temperatures. . . . .  | 35 |
| 34 | Energy requirements of the desorption step of the DAC process versus relative humidity in the bed. Results based on nitrogen regeneration for the proposed adsorption temperature of T = 20°C. . . . .   | 36 |

|    |  |    |
|----|--|----|
| 35 | Energy requirements of the desorption step of the DAC process versus relative humidity in the bed. Results based on steam regeneration for the proposed adsorption temperature of T = 5°C. . . . . | 37 |
| 36 | Fit of the sensor response to ambient conditions to a first order response time function. . . . .  | 46 |
| 37 | Deconvolved RH signal for inlet and outlet measurements of an example experiment. . . . .  | 47 |
| 38 | Sensitivity analysis of energy requirements of the DAC cycle for N <sub>2</sub> regeneration at different values of purge gas flowrate and desorption time. . . . .                                | 48 |
| 39 | Sensitivity analysis of energy requirements of the DAC cycle for steam regeneration at different values of purge gas flowrate and desorption time. . . . .   | 48 |
| 40 | Sensitivity analysis of energy requirements of the DAC cycle for N <sub>2</sub> regeneration at different adsorption step temperatures. . . . .  | 49 |
| 41 | Sensitivity analysis of energy requirements of the DAC cycle for steam regeneration at different adsorption step temperatures. . . . .   | 49 |
| 42 | Two-point linear regression of the C and k parameters of the temperature dependent GAB isotherm model to obtain the parameters $\Delta H_C$ and $\Delta H_k$ . . . . .                             | 50 |

## List of Tables

|   |   |    |
|---|---|----|
| 1 | Physical and chemical properties of Lewatit. . . . .  | 13 |
| 2 | Comparison of water capacity measurements of zeolite UOP 3A for two different values of flowrate using two different measurement methods. . . . . | 21 |
| 3 | Fitting parameters of the theoretical models. . . . .   | 26 |
| 4 | Fitting parameters of the theoretical models. . . . .   | 27 |
| 5 | Fitting parameters of the temperature dependent isotherm model. . . . .   | 29 |
| 6 | Response time constants for the response to ambient conditions. . . . .   | 46 |
| 7 | Physical properties. . . . .  | 47 |
| 8 | Model inputs, unless otherwise stated. . . . .  | 47 |